

# High resolution CMAQ simulations of ozone exceedance events during the Lake Michigan Ozone Study

R. Bradley Pierce<sup>1</sup>, Monica Harkey<sup>4,2</sup>, Allen Lenzen<sup>1</sup>, Lee M. Cronce<sup>3,2</sup>, Jason A. Otkin<sup>1,3,2</sup>, Jonathan L. Case<sup>4,3</sup>, David S. Henderson<sup>1</sup>, Zac Adelman<sup>5</sup>, Tsengel Nergui<sup>5</sup>, Christopher R. Hain<sup>6</sup>

<sup>1</sup>Space Science and Engineering Center, University of Wisconsin-Madison, Madison, 53706, USA

<sup>2</sup>Center for Sustainability and the Global Environment, University of Wisconsin-Madison, Madison, 53706, USA

<sup>3</sup>Cooperative Institute for Meteorological Satellite Studies, University of Wisconsin, Madison, Madison, 53706, USA

<sup>4</sup>ENSCO, Inc., NASA Short-term Prediction Research and Transition Center, Huntsville, 35805, USA

<sup>5</sup>Center for Sustainability and the Global Environment, University of Wisconsin-Madison, Madison, 53706, USA

<sup>6</sup>Lake Michigan Air Directors Consortium, Hillside, 60162, USA

<sup>7</sup>Earth Science Office, NASA Marshall Space Flight Center, Huntsville, 35808, USA

Correspondence to: R. Bradley Pierce ([rbpierce@wisc.edu](mailto:rbpierce@wisc.edu))

**Abstract:** We evaluate two high-resolution Lake Michigan air quality simulations during the 2017 Lake Michigan Ozone Study campaign. These air quality simulations employ identical chemical configurations but use different input meteorology. The “EPA-AP-XM-obs-AP-XM” configuration follows EPA recommended modeling practices, whereas the “YNT\_SSNG” employs different parameterization schemes and satellite-based inputs of sea surface temperatures, green vegetative fraction, and soil moisture and temperature. Overall, we find similar performance in model simulations of hourly and daily 8-hour maximum (MDA8) ozone, with the AP-XM-obs-AP-XMEPA and YNT\_SSNG simulations showing biases of -13.4234 and -13.54 ppbv, respectively during periods when the observed MDA8 was greater than 70ppbv. However, for the two monitoring sites that observed high ozone events, the AP-XM-obs-AP-XMEPA simulation better matched observations at Chiwaukee Prairie Sheboygan-KA and the YNT\_SSNG simulation better matched observations at Sheboygan KA-Chiwaukee-Prairie. We find differences between the two simulations are largest for column amounts of ozone precursors, particularly NO<sub>2</sub>. Across three high ozone events, the YNT\_SSNG simulation has a lower column NO<sub>2</sub> bias (0.17 x 10<sup>15</sup> molecules/cm<sup>2</sup>) compared to the AP-XM-obs-AP-XMEPA simulation (0.3135 x 10<sup>15</sup> molecules/cm<sup>2</sup>). The YNT\_SSNG simulation also has an advantage in better capturing the structure of the boundary layer and lake breeze during the June 2 high ozone event, although the timing of the lake breeze is about 3 hours too early at Sheboygan. Our results are useful in informing an air quality modeling framework for the Lake Michigan area.

## 1. Introduction

Ground-level ozone has many well-documented effects on human health, including increased risk for respiratory and cardiovascular diseases, and even premature death (Di et al., 2017; Lelieveld et al., 2015; Manisalidis et al., 2020). Ozone also damages plant tissue, affecting crop health (e.g. Clifton et al., 2020; Shindell et al., 2012). Ground-level ozone is formed by photochemical reactions between nitrogen oxides (NO<sub>x</sub>) and volatile organic compounds (VOCs); major NO<sub>x</sub> sources include fuel combustion, biomass burning, soil microbes, and lightning, with anthropogenic sources dominant (Hall et al., 1996; Juncosa Calahorrano et al., 2021; Lamsal et al., 2010; Lawrence and Crutzen, 1999; Nault et al., 2017), major sources of VOCs include industrial processes and natural sources, such as trees (Guenther et al., 1995; He et al., 2019).

Since the first National Ambient Air Quality Standard (NAAQS) for ozone was released in 1979, most lakeshore counties in the states bordering Lake Michigan (Wisconsin, Illinois, Indiana, and Michigan) have been designated as being in nonattainment for surface ozone in one or more of the subsequent NAAQS revisions. These states are required by the Clean Air Act to develop State Implementation Plans (SIPs) to demonstrate strategies to bring affected areas into attainment and to mitigate the impacts of high ozone concentrations. Large decreases in local emissions of ozone

49 precursors have steadily reduced one- and eight-hour maximum ozone concentrations across the region in recent  
50 decades (Adelman 2020). However, the implementation of stricter ozone NAAQS, along with increases in susceptible  
51 populations (e.g. Daggett et al., 2000), means that additional air quality modeling assessments are necessary to help  
52 states demonstrate that they can reach attainment by the required statutory deadlines.  
53

54 The areas along the Lake Michigan shoreline are susceptible to high ozone amounts because of a combination of  
55 abundant precursor emissions and transport processes, particularly the lake breeze circulation. The relationships  
56 between area emissions and meteorology as they impact air quality [along the Lake Michigan shoreline](#) have been  
57 characterized in field campaigns (Sexton and Westberg, 1980; Dye et al., 1995; Foley et al., 2011; Stanier et al., 2021),  
58 and the meteorological component is the subject of Part I of this study (Otkin et al., 2023). Ozone concentrations  
59 along coastlines can be enhanced significantly when urban emissions react within the shallow, stable, marine boundary  
60 layer (Fast and Heilman, 2003). The lake breeze circulation is particularly important for enhanced ozone production  
61 over Lake Michigan where it contributes to roughly 80% of high ozone episodes observed in eastern Wisconsin  
62 (Lennartson and Schwartz, 2002; Cleary et al., 2021). [Lake breeze circulations impact ozone concentrations elsewhere  
63 in the Great Lakes including southern Ontario, Michigan, and Ohio \(Makar et al. 2010, He et al., 2011, Brook et al.  
64 2013, Stroud et al. 2020\).](#)

65  
66 As highlighted by Dye et al. (1995), there has been a need for a modeling framework that represents the finer scales  
67 of emissions transport and chemistry near the Lake Michigan shoreline. [It is our opinion that d](#)Developing emission  
68 control strategies to mitigate these coastal high ozone events requires accurate prediction of the lake breeze transport  
69 processes at scales of 1-10 km. [Furthermore, t](#)These chemical transport processes cannot be accurately resolved using  
70 the 12-km resolution meteorological and chemical simulations typically used in air quality modeling for previous  
71 SIPs.  
72

73 We have developed a high-resolution, satellite-constrained meteorological modeling platform for the Midwest United  
74 States that supports the needs of the Lake Michigan Air Directors Consortium (LADCO) as they conduct detailed air  
75 quality modeling assessments for its member states. In part I of this study, Otkin et al. (2023) assessed the impact of  
76 different high-resolution surface datasets, parameterization schemes, and analysis nudging on near-surface  
77 meteorological conditions and energy fluxes relative to the model configuration and input datasets typically employed  
78 by the Environmental Protection Agency (EPA). In part II of this study, we use meteorological output obtained from  
79 two of these simulations, as input to the EPA Community Multiscale Air Quality (CMAQ) model version 5.2.1 (Byun  
80 and Schere, 2006; Nolte et al., 2015) model simulations to assess the impact of these model changes on ozone forecasts  
81 in the Lake Michigan region. The remainder of this paper is organized as follows: Section 2 contains a description of  
82 the CMAQ model configurations and observational data used for evaluation. Results are presented in Section 3, with  
83 discussion and conclusions provided in Section 4.

## 84 2. Methods

85 In this work, we compare two CMAQ simulations, one with [AP-XM-obsbaseline EPA](#) meteorology, and the other  
86 with meteorology from our optimized WRF configuration, [as as](#)-detailed in Part I (Otkin et al., 2023). Both sets of  
87 meteorological simulations employ a triple-nested domain configuration containing 12-, 4-, and 1.33333 (1.3)-km  
88 resolution grids, respectively (Figure 1 in Otkin et al., 2023), [constrained to 6-hourly, 0.25-degree GFS Final  
89 reanalyses and as well as using](#) RRTMG longwave and shortwave radiation (Iacono et al. 2008; Mlawer et al. 1997)  
90 [on all three domains, and](#) the Kain-Fritsch cumulus scheme (Kain 2004) on the outer two domains, [and explicit  
91 convection on the innermost domain. Both simulations have the same vertical resolution throughout, with 6 model  
92 layers below 200m, 4 model layers below 100m, and the lowest three layers at ~9, 27, and 55m above ground level.](#)  
93 The [AP-XM-obsAP-XMEPA](#) simulation employs the Morrison microphysics (Morrison et al. 2005), ACM2 PBL  
94 (Pleim 2007), and the Pleim-Xu LSM (Gilliam and Pleim 2010; Xiu and Pleim, 2001) parameterization schemes,  
95 [which are the same schemes used within CMAQ and is therefore considered our baseline meteorological simulation,  
96 with indirect soil moisture and soil temperature nudging and nudging to surface observations of humidity, sea level  
97 pressure, temperature and wind from the Meteorological Assimilation Data Ingest System \(MADIS,  
98 <https://madis.ncep.noaa.gov/>\).](#) Our optimized meteorological modeling platform uses the YSU PBL (Hong et al.  
99 2006), Noah LSM (Chen and Dudhia, 2001; Ek et al. 2003), and Thompson microphysics (Thompson et al. 2008,  
100 2016) schemes, constrained by high-resolution (1km) soil moisture and temperature analyses (Case 2016; Case and  
101 Zavodsky 2018; Blankenship et al. 2018) from the Short-term Prediction Research and Transition Center (SPoRT),

102 daily high resolution (1.3 km) Great Lakes surface temperatures (Schwab 1992) from the Great Lakes Surface  
103 Environmental Analysis (GLSEA), and high resolution (4 km) Green Vegetation Fraction (GVF) from the Visible  
104 Infrared Imaging Radiometer Suite (VIIRS; Vargas et al. 2015) in place of monthly GVF climatologies. This  
105 optimized configuration is hereafter referred to as the YNT\_SSNG. Otkin et al. (2023) found that the [AP-  
106 XM-obsAP-XMEPA](#) configuration generally produced more accurate meteorological analyses on the 12-km domain,  
107 but its accuracy decreased with finer model grid resolution. In contrast, the YNT\_SSNG statistics showed consistent  
108 reductions in [root-mean-square error \(RMSE\)](#) for 2-m temperature, 2-m water vapor mixing ratio, and 10-m wind  
109 speed relative to the [AP-XM-obsAP-XMEPA](#) as the model resolution increased from 12 km to 1.3 km. [We note that  
110 differences in near surface wind speed and GVF will also impact deposition velocities in the CMAQ simulations.](#)

112 Each CMAQ simulation is run with the same configuration and anthropogenic emissions. [Using CMAQv5.2.1  
113 \(Appel et al., 2017; US EPA, 2018\)](#), our configuration includes "AERO6" aerosol chemistry, the Carbon Bond 6  
114 chemical mechanism [revision 3 \(CB6r3; Emery et al., 2015; Luecken et al., 2019\)](#), and in-line photolysis. CMAQ  
115 was run with 39 vertical layers with a top of approximately 100 hPa, thus using all available layers from our WRF  
116 simulations. As with our WRF simulations, we ran CMAQ on three domains: one using 12 km by 12 km horizontal  
117 resolution over the continental U.S. (396 x 246 grid points), one using 4 km by 4 km horizontal resolution over the  
118 upper Midwest (447 x 423 grid points), and one using 1.3 km by 1.3 km horizontal resolution over Lake Michigan  
119 and nearby areas (245 x 506 grid points). The 12 km CMAQ simulations employ lateral boundary conditions ([LBC](#))  
120 from the [global Real-time Air Quality Modeling System \(RAQMS\) model \(Pierce et al., 2007\)](#), which includes  
121 assimilation of ozone retrievals from the Microwave Limb Sounder (MLS) and Ozone Monitoring Instrument (OMI)  
122 on the NASA Aura satellite and assimilation of aerosol optical depth (AOD) from the Moderate Resolution Imaging  
123 Spectroradiometer (MODIS) on the NASA Terra and Aqua satellites. [Utilizing RAQMS LBC for CMAQ  
124 continental scale simulations has been shown to significantly increase upper tropospheric ozone and improve daily  
125 maximum surface O<sub>3</sub> concentrations \(Song et al., 2008\) and improve agreement with OMI tropospheric ozone  
126 column \(Lee et al. 2012\) relative to fixed LBC.](#) The 4-km and 1.3-km simulations employ lateral boundary  
127 conditions from the respective parent grid.

129 Anthropogenic emissions for the 12 km domain were taken from the 2016 National Emissions Inventory Collaborative  
130 (NEIC, 2019), version 1. Anthropogenic emissions for the 4 km and 1.3 km domains were taken from the 2017  
131 National Emissions Inventory, version 1 (US EPA, 2021; Adams, 2020), where emissions on the 4 km domain were  
132 provided by the EPA (Kirk Baker, personal communication), and then interpolated and downscaled -by 1/9<sup>th</sup> for use  
133 on the 1.3 km domain. [We acknowledge that the use of downscaled 4km emissions will degrade the performance of  
134 the 1.3km simulations, but generating 1.3km area emissions from the Sparse Matrix Operator Kernel Emissions  
135 \(SMOKE\) programs was beyond the scope of this project.](#) Biogenic emissions were calculated [in-line](#) using the  
136 Biogenic Emission Inventory System (BEIS) with the Biogenic Emissions Landuse Database, version 3 (BELD3;  
137 Carlton and Baker, 2011). Meteorologically-sensitive input for ~~in-line~~ biogenic emissions calculations (such as frost  
138 dates) were generated separately for each set of CMAQ simulations using ~~Sparse Matrix Operator Kernel Emissions~~  
139 (SMOKE) programs. As biogenic emissions are calculated in-line, they vary among our configurations with differing  
140 input [meteorology and GVF](#).

142 We focus on the innermost, 1.3 km domain surrounding Lake Michigan, during the 2017 Lake Michigan Ozone Study  
143 (LMOS) field campaign (Stanier et al., 2021) which occurred from 22 May –22 June 2017. Our chemical evaluation  
144 focuses on ozone and ~~three~~two of its precursors, nitrogen dioxide, ~~and~~ formaldehyde [and isoprene](#), in the surface layer  
145 and in the atmospheric column. We employ ozone observations from the Air Quality System (AQS) monitoring  
146 network, using the Atmospheric Model Evaluation Tool (AMET) developed by the EPA. We also utilize nitrogen  
147 dioxide (NO<sub>2</sub>) and formaldehyde (HCHO) in situ observations from an EPA trailer that was deployed at Sheboygan,  
148 WI, and [NO<sub>2</sub> and isoprene measurements from the LMOS Zion supersite \(Stanier et al., 2021\)](#). In situ O<sub>3</sub> and wind  
149 observations at select monitors that were submitted to the LMOS data repository  
150 (<https://asdc.larc.nasa.gov/soot/power-user/LMOS/2017>). For column evaluation, we employ observations of column  
151 NO<sub>2</sub> and HCHO from the Geostationary Trace Gas Aerosol Sensor Optimization (GeoTASO; Leitch et al., 2014)  
152 instrument taken during LMOS (Judd et al., 2019).

### 153 3. Results

Formatted: Left, Don't adjust space between Latin and Asian text, Don't adjust space between Asian text and numbers

Formatted: Font: (Default) Times New Roman

Formatted: Font: (Default) Times New Roman, Subscript

Formatted: Font: (Default) Times New Roman

Formatted: Font: (Default) AdvTT5843c571, Font color: Auto

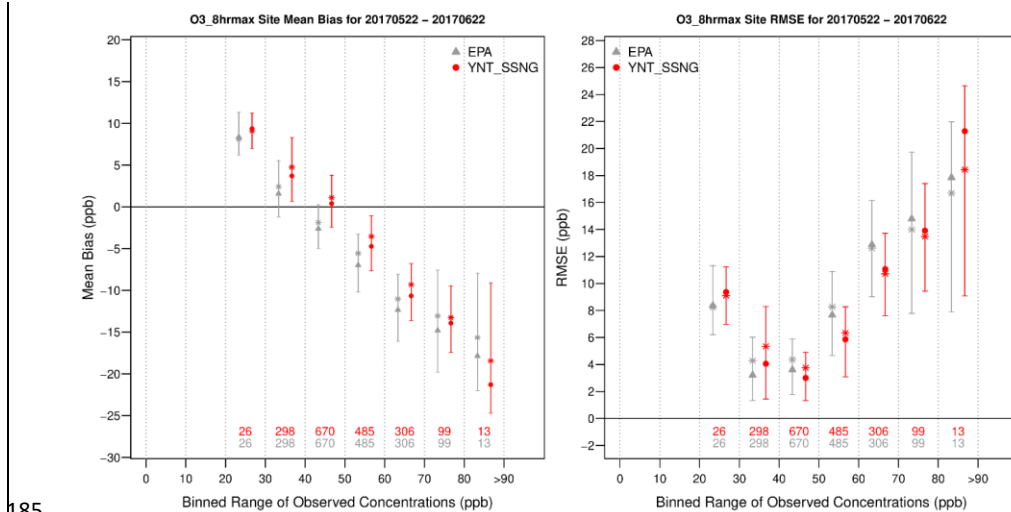
154 Our model comparison is organized by three time periods. We first evaluate model performance of the ~~AP-~~  
 155 ~~XM\_obsAP-XM~~EPA and YNT\_SSNG simulations over the entire LMOS period, based on the ozone precursors of  
 156 NO<sub>2</sub> and HCHO, and isoprene as well as daily 8-h maximum ozone. Used in the NAAQS for ozone, maximum 8-  
 157 hour ozone amounts are calculated as a rolling 8-h average for each day, starting for the period of 7 am to 3 pm local  
 158 standard time (LST), and ending with the period of 11 pm to 7 am LST the following day. However, 8-h maximum  
 159 ozone is strongly influenced by days with low and moderate ozone concentrations. Though only 5.9% (112) of the 8-  
 160 hour maximum ozone periods within the 1.3 km domain were above the NAAQS threshold for ozone (70 ppbv) during  
 161 LMOS (see Fig. -1), it is these higher 8-h maximum ozone values that are most relevant to SIP modeling.  
 162

163 To evaluate the simulations more precisely, we then evaluate the high ozone days as identified by the two coastal AQS  
 164 monitors that tend to show the highest ozone concentrations. High ozone days with extensive observations during  
 165 LMOS 2017 include: 2-4 June, 9-12 June, and 14-16 June (Abdi-Oskouei et al., 2020) and are referred to as events  
 166 A, B, and C, respectively. Finally, we evaluate model performance over the broader western Lake Michigan shoreline  
 167 area during the only ozone exceedance event on 2 June.

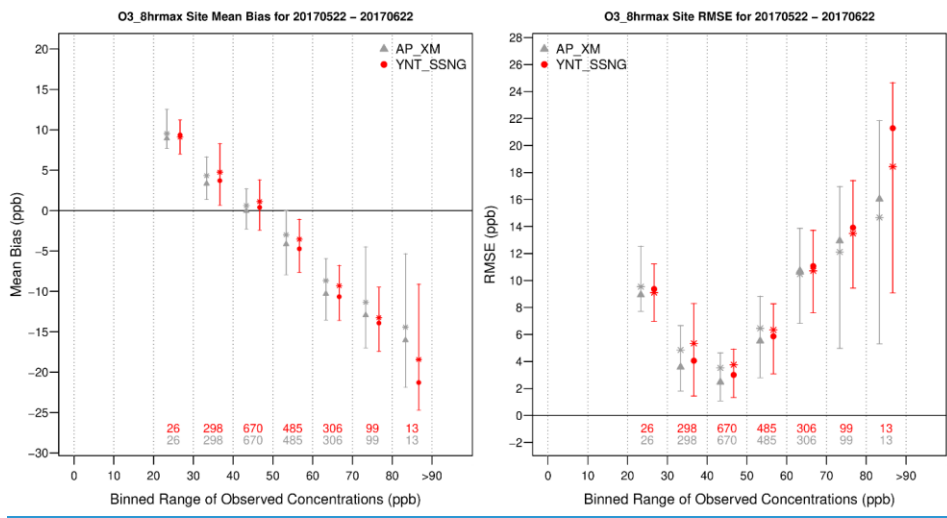
### 168 3.1 Model performance over the entire LMOS period

#### 169 3.1.1 8-hour maximum ozone

170 Figure 1 shows binned whisker plots of 8-h maximum ozone bias and RMSE at 10 ppb intervals for the 1.3km  
 171 simulations for all sites within the 1.3km domain. Systematic high biases for lower ozone concentrations (< ~40 ppbv)  
 172 and a low bias for higher ozone concentrations (> 50 ppbv) are evident in both simulations. ~~However, the~~  
 173 ~~YNT\_SSNG and AP-XM simulations show similar smaller biases and RMSE than the AP-XM\_obsEPA for 8-h~~  
 174 ~~maximum ozone concentrations between 40-870 ppbv, but Both simulations show similar biases and RMSE within~~  
 175 ~~the 70-80 ppbv bin and the AP-XM\_obsAP-XM~~EPA shows significantly lower biases and RMSE in the 80-90 ppbv  
 176 bin. Figure 2 shows the geographical distribution of 8-h maximum ozone bias and RMSE for the 1.3km ~~AP-~~  
 177 ~~XM\_obsAP-XM~~EPA and YNT\_SSNG for all AQS sites within the 1.3km domain. Overall biases are largely negative,  
 178 reflecting underestimates of 8-h maximum ozone at the AQS sites. When compared on a site-by-site basis, the biases  
 179 and RMSE in 8-h maximum ozone are generally smaller by more than 2 ppbv in the YNT\_SSNG simulation ~~with the~~  
 180 ~~exception of two AQS sites in North Chicago where the YNT\_SSNG simulations shows overestimates of 4-8 ppbv in~~  
 181 ~~8-h maximum ozone. This may be due to the use a more realistic, and lower (relative to climatology) Green~~  
 182 ~~Vegetation Fraction (see Figure 2 in Otkin et al., 2023) in the YNT\_SSNG simulation which would tend to reduce~~  
 183 ~~ozone deposition velocities and increase ozone concentrations (Ran et al., 2016).~~  
 184

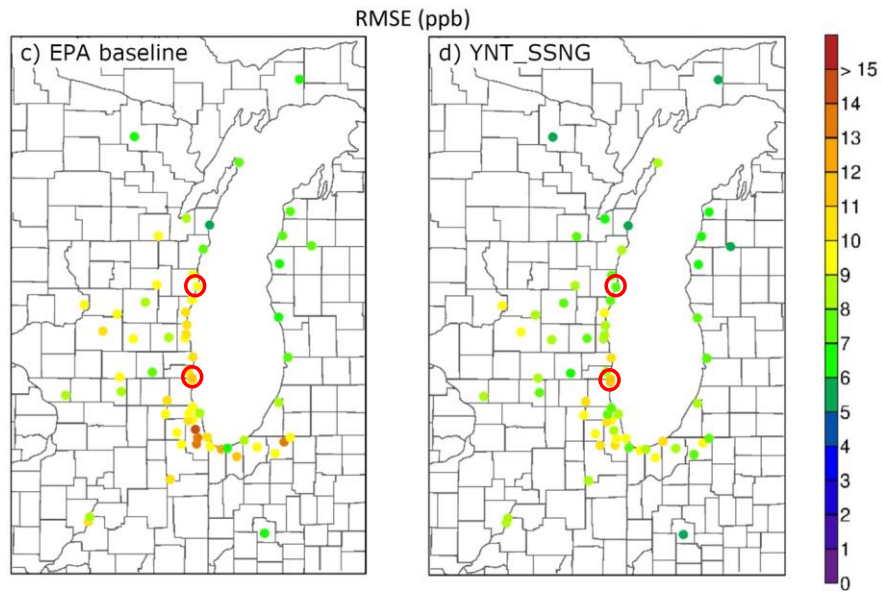
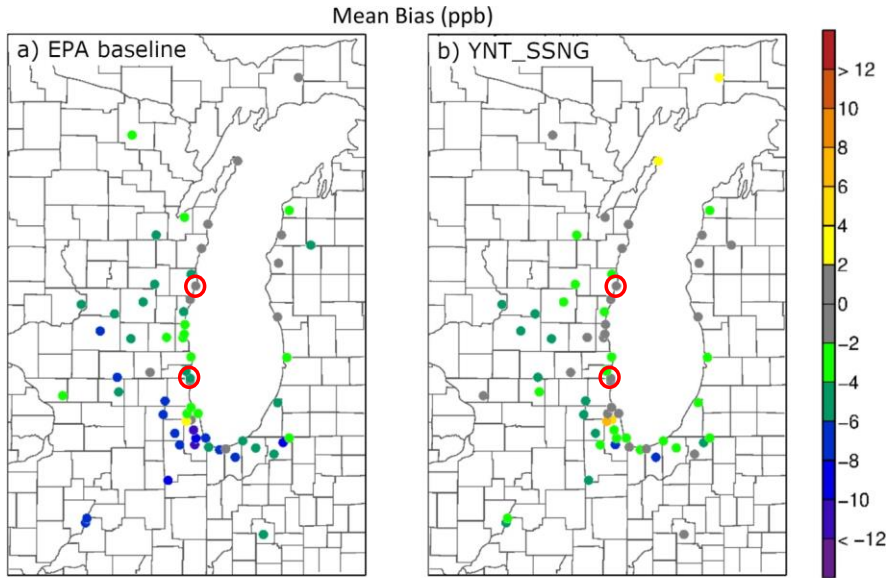


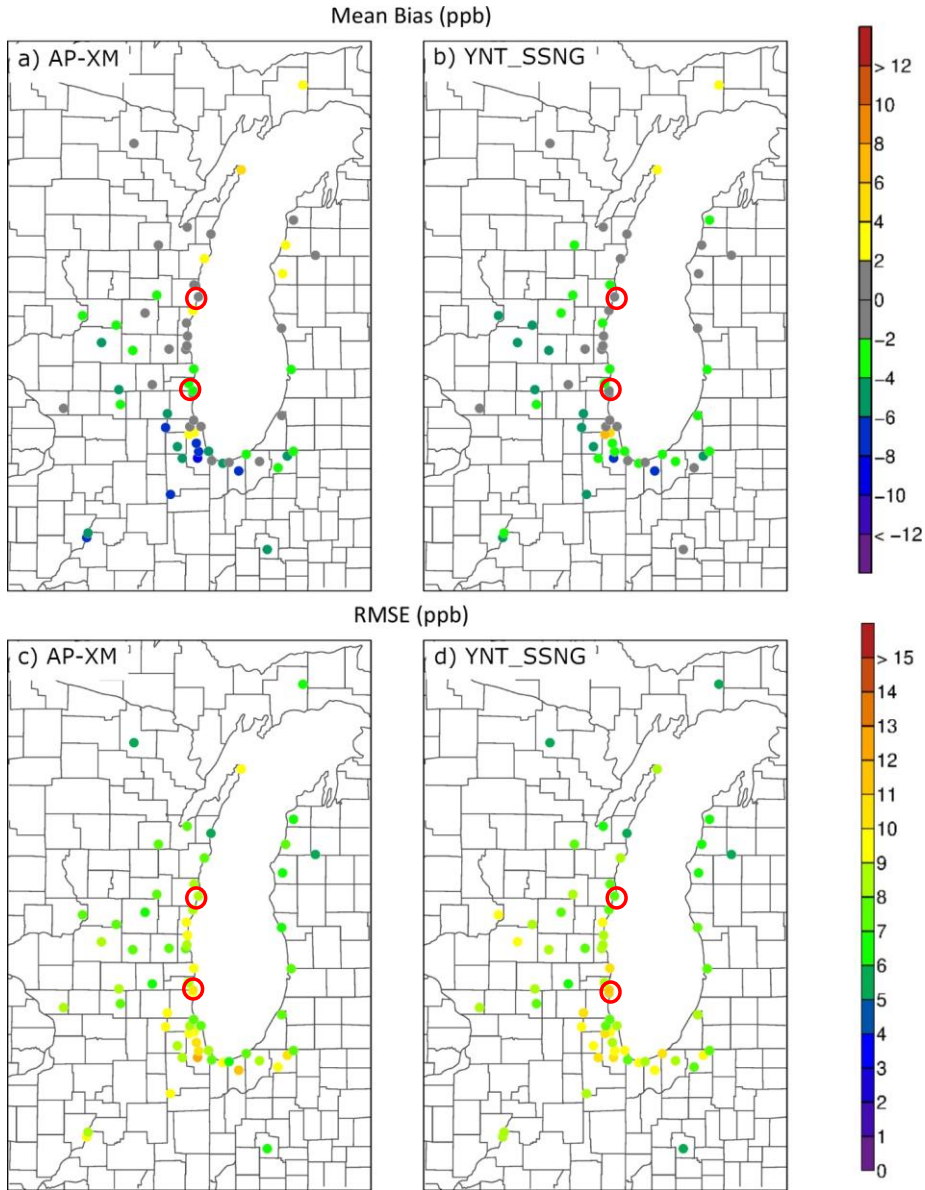
185



186  
 187 **Figure 1. Whisker plots showing the bias (left) and RMSE (right) for binned 8-h maximum ozone concentrations from the**  
 188 **AP\_XM\_obsAP\_XMEPA (gray) and YNT\_SSNG (red) CMAQ simulations using hourly data within the 1.3km domain**  
 189 **during the LMOS period of record from 22 May 2017 to 22 June 2017. Triangles and circles represent the conditional**  
 190 **distribution medians, stars represent distribution means, and lines and whiskers represent the Q1 to Q3 ranges.**

191





193  
 194  
 195  
 196  
 197  
 198

Figure 2. Geographical distribution of bias (upper panels) and RMSE (lower panels) for binned 8-h maximum ozone concentrations from the AP-XM-obsAP-XMEPA (left) and YNT\_SSNG (right) 1.3km CMAQ simulations using hourly data from all stations in the 1.3 km resolution inner during the LMOS period of record from 22 May 2017 to 22 June 2017. Bias and RMSE (ppbv) at each site are indicated by the color bar. Two AQ5 monitors, Sheboygan KA to the north and Chiwaukee Prairie along the Wisconsin-Illinois border are indicated by the red circles.

199

200 **3.1.2 Evaluation with Sheboygan WI ground-based NO<sub>2</sub> and HCHO measurements**

201 During LMOS, the EPA deployed instruments measuring in-situ NO<sub>2</sub> and HCHO in Sheboygan, WI to characterize  
202 ozone precursors along the shore of Lake Michigan. These 1-min measurements were taken at Spaceport Sheboygan,  
203 which is approximately 9 km north of the Sheboygan, KA monitor highlighted in Figure 2. Here, we use the hourly  
204 averaged EPA NO<sub>2</sub> and HCHO measurements to evaluate the accuracy of prediction of ozone precursors at Sheboygan  
205 for the YNT\_SSNG and AP-XM\_obsAP-XMEPA CMAQ simulations.

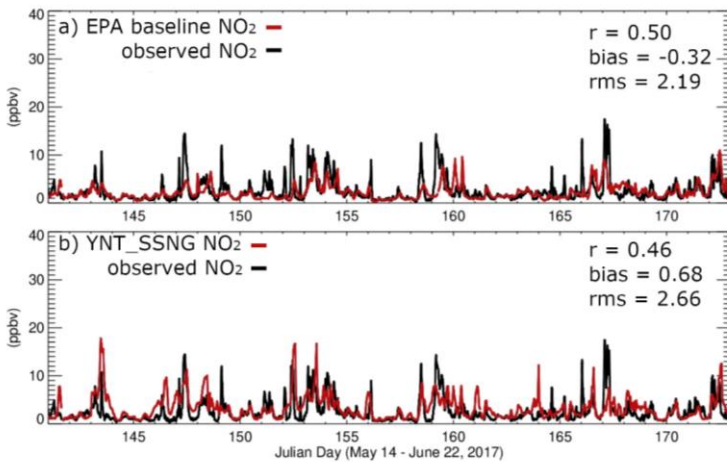
206  
207 Figures 3 and 4 show the hourly NO<sub>2</sub> and HCHO comparisons, respectively. There are several periods where observed  
208 NO<sub>2</sub> (black lines, Figure 3) is above 10 ppbv; these periods are generally underestimated by the AP-XM\_obsAP-  
209 XMEPA simulation and overestimated by the YNT\_SSNG simulation (red lines, Figure 3). We find an overall slight  
210 positive/negative bias of -0.19/3.2 ppbv for the AP-XM\_obsAP-XMEPA and an overall positive bias of 0.68 ppbv for  
211 the YNT\_SSNG simulation. We also find that the correlations are slightly lower and RMS errors are slightly higher  
212 in the YNT\_SSNG simulation than in the AP-XM\_obsAP-XMEPA simulation.

213  
214 Observed HCHO shows peak amounts in excess of 4 ppbv (black lines, Figure 4) which are underestimated in both  
215 simulations (red lines, Figure 4). However, the YNT\_SSNG simulation tends to have overall higher HCHO mixing  
216 ratios than the AP-XM\_obsAP-XMEPA simulation leading to a nearly 50% reduction (-0.26 versus -0.54/3.4 ppbv) in  
217 the low bias relative to the EPA measurements. This is in spite of the fact that the YNT\_SSNG uses a more realistic,  
218 and lower (relative to climatology) Green Vegetation Fraction (see Figure 2 in Otkin et al. 2023) which would tend to  
219 reduce biogenic VOC emissions. This suggests that anthropogenic VOC emissions may be playing a role in the  
220 reduction of the low biases in the YNT\_SSNG simulation. This is likely due to the incorporation of more realistic  
221 (relative to climatology) GVF observations in the YNT\_SSNG simulation and better representation of biogenic VOCs.  
222 Compared to the AP-XM\_obsAP-XMEPA simulation, we also find correlations and RMS errors are slightly lower in  
223 the YNT\_SSNG simulation.

224  
225 The larger high biases in NO<sub>2</sub> and reduced low biases in HCHO in the YNT\_SSNG simulation leads to significant  
226 reductions in high biases in ozone in the YNT\_SSNG compared to the AP-XM simulation (0.07 versus 1.76 ppbv,  
227 not shown) and may be due to more nighttime ozone titration in the YNT\_SSNG simulation.

Formatted: Subscript

228

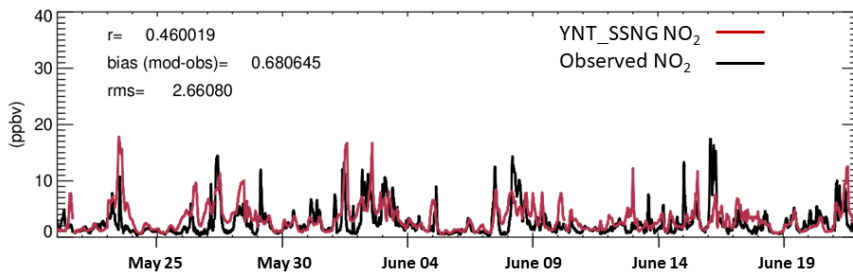
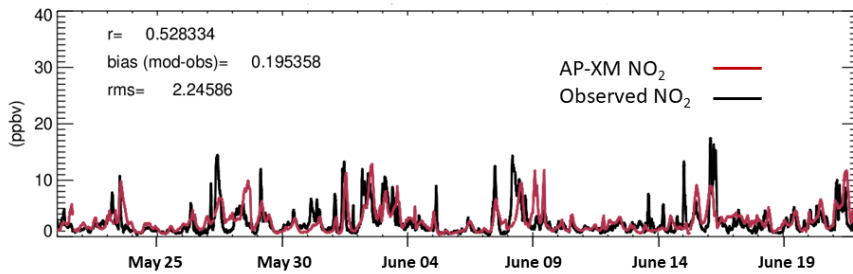


229

230

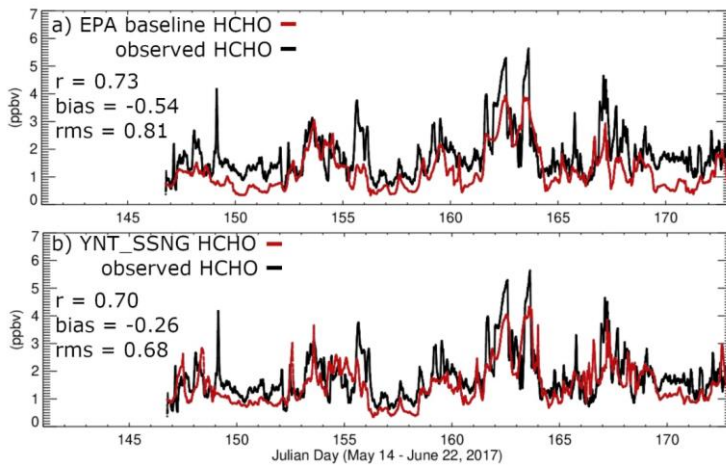
231





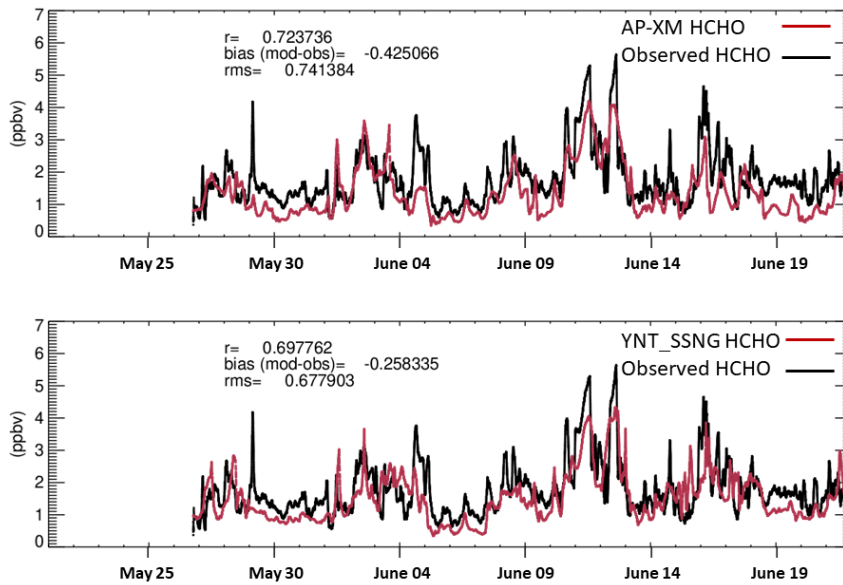
232  
233  
234  
235  
236  
237  
238

Figure 3: Timeseries of 1-hour averaged NO<sub>2</sub> at Spaceport Sheboygan for the 1.3km AP-XM-obsAP-XMEPA (upper) and YNT\_SSNG (lower) CMAQ simulations (red) and EPA observations (black) during the LMOS 2017 time period (May 22-June 21, 2017).



239

240  
241



242  
243 **Figure 4:** Timeseries of 1-hour averaged HCHO at Spaceport Sheboygan for the 1.3km ~~AP-XM-obs~~AP-XMEPA (upper)  
244 and YNT\_SSNG (lower) CMAQ simulations (red) and EPA observations (black) during the LMOS 2017 time period (May  
245 22-June 21, 2017).

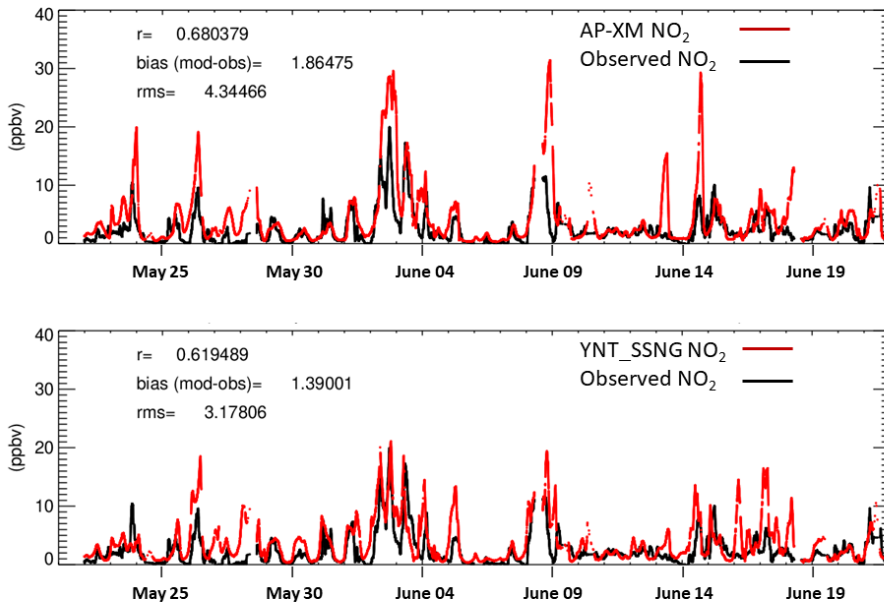
246 **3.1.3 Evaluation with Zion IL ground-based NO<sub>2</sub> and iSoprene measurements**

247 [During LMOS, the University of Wisconsin deployed a Thermo Scientific NO-NO2-NO2 Analyzer Model 42i](#)  
248 [instrument measuring in-situ NO<sub>2</sub> and the University of Minnesota deployed a Proton-Transfer Quadrupole Interface](#)  
249 [Time-Of-Flight Mass Spectrometer \(PTR-QiTOF\) measuring iSoprene at the LMOS Zion ground site to characterize](#)  
250 [ozone precursors along the shore of Lake Michigan. These 1-min measurements were co-located at the Illinois Air](#)  
251 [Monitoring site \(17-097-1007\) in Illinois Beach State Park, which is approximately 4 km south of the Chiwaukee](#)  
252 [monitor highlighted in Figure 2. Here, we use the hourly averaged NO<sub>2</sub> and iSoprene measurements to evaluate the](#)  
253 [accuracy of prediction of ozone precursors at Zion for the YNT\\_SSNG and AP-XM CMAQ simulations.](#)

254  
255 [Figures 5 and 6 show the hourly NO<sub>2</sub> and iSoprene comparisons, respectively. There are several periods where](#)  
256 [observed NO<sub>2</sub> \(black lines, Figure 5\) is above 10 ppbv; these periods are generally overestimated by the AP-XM](#)  
257 [simulation with YNT\\_SSNG simulation in much better agreement with observations \(red lines, Figure 5\). We find an](#)  
258 [overall positive bias of 1.86 ppbv for the AP-XM and an overall positive bias of 1.39 ppbv for the YNT\\_SSNG](#)  
259 [simulation. We also find that the correlations are slightly lower and RMS errors are lower in the YNT\\_SSNG](#)  
260 [simulation than in the AP-XM simulation.](#)

261  
262 [Observed iSoprene shows peak amounts in excess of 4 ppbv \(black lines, Figure 6\) which are significantly](#)  
263 [underestimated in both simulations \(red lines, Figure 6\). The YNT\\_SSNG simulation tends to have overall lower](#)  
264 [iSoprene mixing ratios than the AP-XM simulation leading to a larger low bias \(-0.34 versus -0.28 ppbv\) for the](#)

265 [YNT\\_SSNG simulation relative to the Zion measurements. This is consistent with the use of more realistic, and lower](#)  
 266 [\(relative to climatology\) Green Vegetation Fraction in the YNT\\_SSNG simulation \(see Figure 2 in Otkin et al. 2023\).](#)  
 267 [We also find correlations with observed isoprene are higher and RMS errors are slightly higher in the YNT\\_SSNG](#)  
 268 [simulation.](#)  
 269



270 [Figure 5: Timeseries of 1-hour averaged NO<sub>2</sub> at Zion for the 1.3km AP-XM \(upper\) and YNT\\_SSNG \(lower\) CMAQ](#)  
 271 [simulations \(red\) and observations \(black\) during the LMOS 2017 time period \(May 21-June 22, 2017\).](#)  
 272  
 273

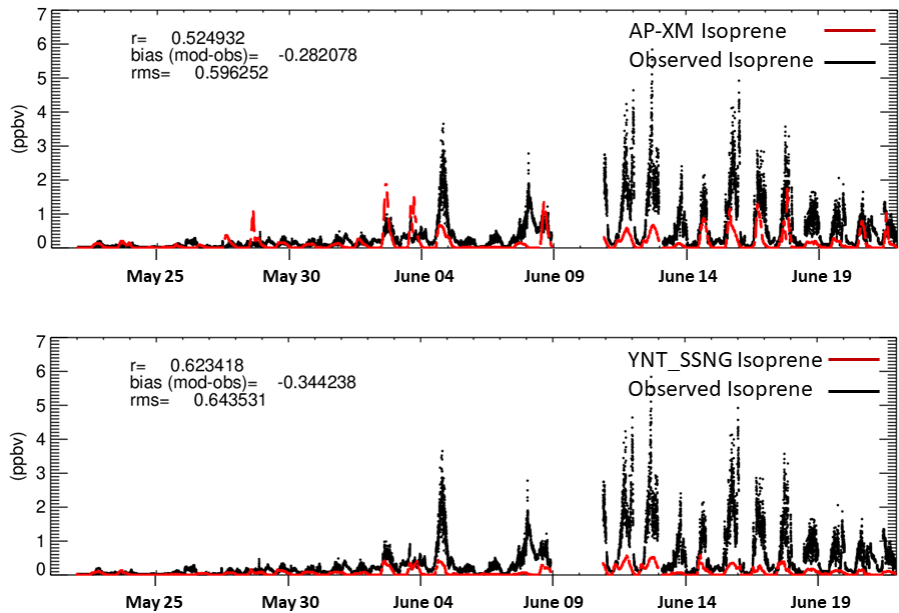


Figure 6: Timeseries of 1-hour averaged Isoprene at Zion for the 1.3km AP-XM (upper) and YNT\_SSNG (lower) CMAQ simulations (red) and observations (black) during the LMOS 2017 time period (May 21-June 22, 2017).

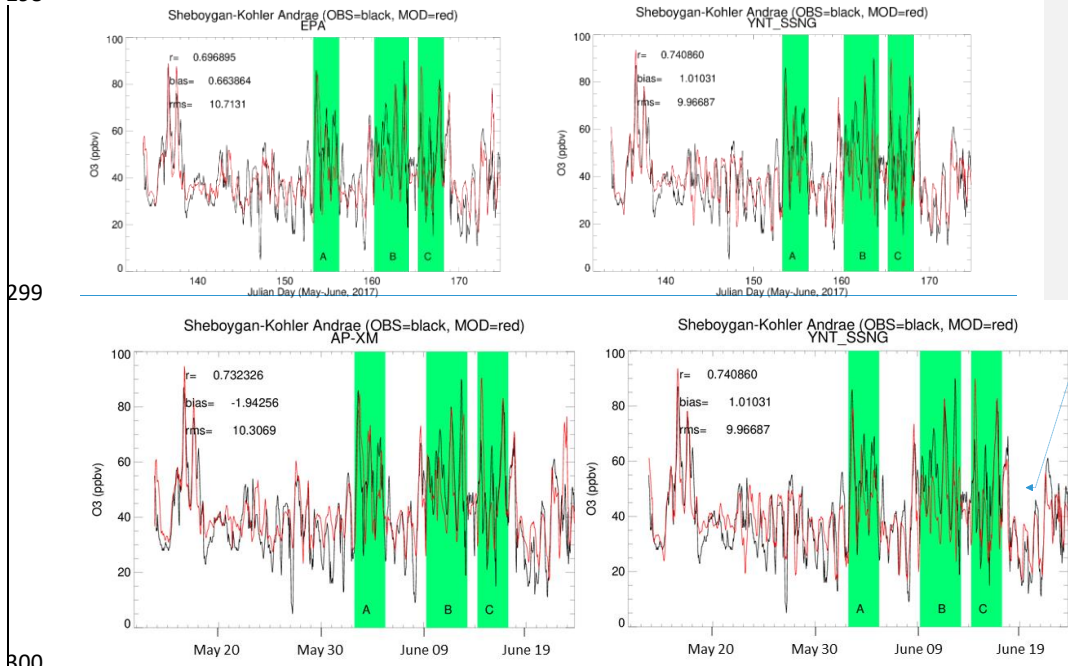
### 3.2 Model performance during high-ozone events

#### 3.2.1 Sheboygan KA and Chiwaukee Prairie 1-hour ozone

In this and the following sections, we focus on the two AQS monitors that showed high ozone events during LMOS most clearly: the Sheboygan Kolher Andrae (KA) monitor (AQS 551170006), located south of Sheboygan, WI, and the Chiwaukee Prairie monitor (AQS 550590019) is located near the Wisconsin/Illinois border. These two sites are indicated by red circles in Figure 2.

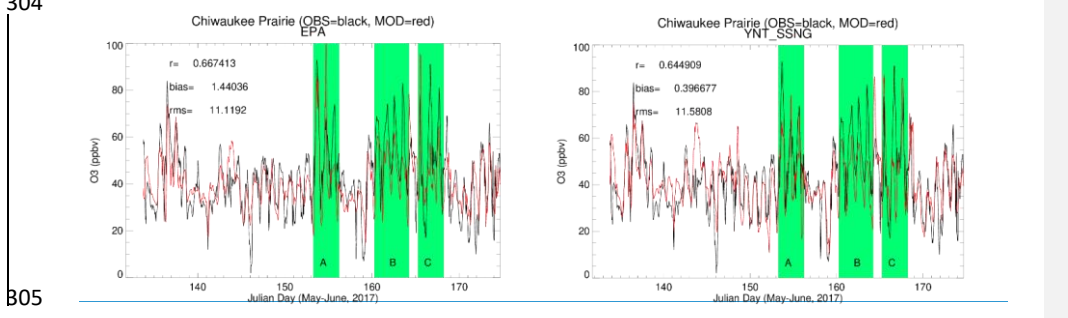
Figures 75 and 86 show the hourly AQS observed and CMAQ AP-XM\_obsAP-XMEPA and YNT\_SSNG simulated O<sub>3</sub> for Sheboygan KA and Chiwaukee Prairie monitors. Comparisons with AQS observations and the two simulations at Sheboygan KA show similar increased correlations (0.744 versus 0.73697), reduced increased biases (1.01 versus -1.90.664 ppbv) and similar reduced RMSE (9.97 versus 10.37 ppbv) for the YNT\_SSNG relative to the AP-XM simulation. Similar comparisons at Chiwaukee Prairie show decreased correlations (0.64 versus 0.7067), higher reduced biases (0.4397 versus -0.131.44 ppbv) and increased RMSE (11.58 versus 11.5812 ppbv) for the YNT\_SSNG relative to the AP-XM simulation. Student T-Tests between the AP-XM and YNT\_SSNG simulations at each site show that the simulations have statistically significant differences (99% confidence level) in mean ozone concentration at Sheboygan KA but not at Chiwaukee Prairie. While the overall hourly ozone statistics at Sheboygan KA and Chiwaukee Prairie are relatively similar between the AP-XM\_obsAP-XMEPA and YNT\_SSNG simulations

296 at these sites, the simulations during high ozone events are quite different. This is illustrated by looking at composite  
 297 statistics during events A, B, and C.  
 298



Formatted: Centered

300  
 301 **Figure 75:** Timeseries of 1-h ozone at Sheboygan-Kohler Andrae AQS monitor (551170006) for the 1.3km ~~AP\_XM-obsAP-~~  
 302 ~~XMEPA~~ (left) and YNT\_SSNG (right) CMAQ simulations (red) and AQS observations (black) during the LMOS 2017 time  
 303 period (May 22-June 21, 2017). The green highlighting shows the periods of high ozone events A, B, and C.  
 304



305

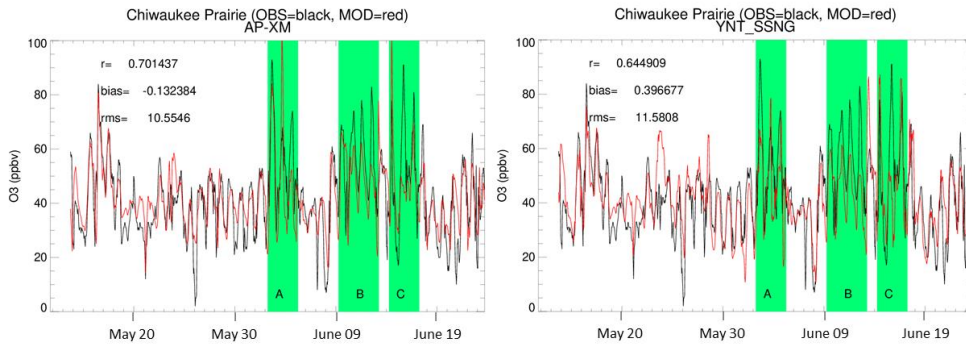


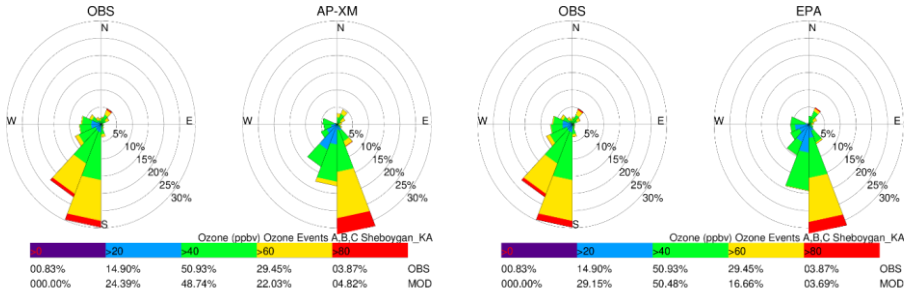
Figure 86: Same as in Figure 5 but for Chiwaukee Prairie AQS monitor (550590019).

### 3.2.2 Composite ozone wind roses during high ozone events A, B, C

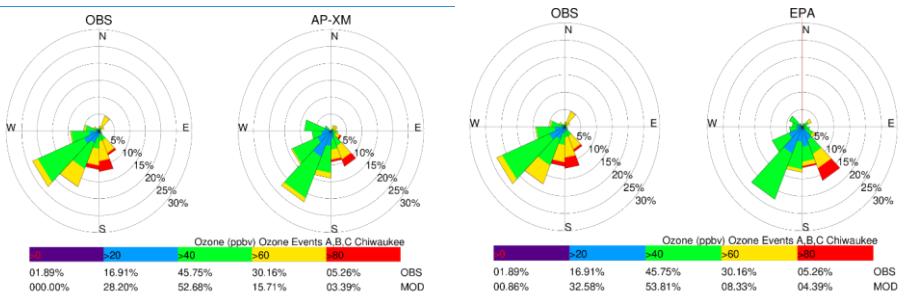
Figure 97 shows observed and simulated composite ozone wind roses from the 1.3km AP-XM-obsAP-XMEPA and YNT\_SSNG simulations at the Sheboygan KA and Chiwaukee Prairie monitors during high ozone events A, B, and C. At Sheboygan KA, the observed wind direction is most frequently (>50%) from the south-southwest (SSW), which is also the direction where the majority of the higher (>60ppbv) ozone is observed during south-southeast (SSE) ozone events. The AP-XM-obsAP-XMEPA simulation predicts winds which are most frequently (>30%) from the south-southeast (SSE) with the majority of the higher ozone coming from this direction. The YNT\_SSNG simulation predicts winds which are more variable but also most frequently (>20%) from the SSE with most of the higher ozone coming from this direction. The overall frequency of higher ozone in the AP-XM-obsAP-XMEPA simulation (~27%) is closer to the observed percentage (~33%) than the YNT\_SSNG simulation (~15%). These comparisons show that the AP-XM-obsAP-XMEPA meteorology best captures the observed ozone wind rose at Sheboygan KA during high ozone events.

At Chiwaukee Prairie the observed winds are more variable and are most frequently (>40%) from the southwest. While some of the observed higher ozone comes from the southwest, the highest (> 80 ppbv) ozone comes from the SSE. Both the AP-XM-obsAP-XMEPA and YNT\_SSNG simulations frequently predict southwest winds (~30% and ~50%, respectively) with lower ozone (< 60 ppbv) than observed. Both the AP-XM-obsAP-XMEPA and YNT\_SSNG simulations show the highest ozone coming from the SSE, but the AP-XM-YNT\_SSNG simulation more accurately captures the observed percentages of high ozone coming from the SSE while AP-XM-obsEPA simulation shows both low and high ozone coming from the southeast at Chiwaukee Prairie. The overall frequency of higher ozone in the AP-XM-obsAP-XMEPA (~19%) and YNT\_SSNG (~13%) are both lower than and YNT\_SSNG simulations are very similar (~13%) and both underestimate the observed percentage (~35%), however, most of the higher ozone in the AP-XM-obsEPA simulation comes from the southeast. These comparisons show that the AP-XM-YNT\_SSNG simulation best captures the observed ozone wind rose at Chiwaukee Prairie during high ozone events but that both simulations have a low bias in ozone when winds are from the southwest.

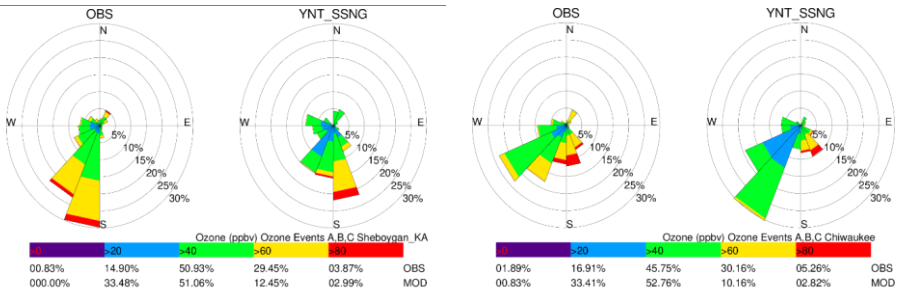
334



335



336



337

338

339

340

341

342

343

344

Figure 97: Observed (OBS) and simulated wind roses using 1-h ozone and wind directions at the Sheboygan-Kohler Andrae AQS monitor (551170006, left columns) and Chiwaukee Prairie AQS monitor (550590019, right columns) for the 1.3km AP\_XM\_obs/AP\_XMEPA (upper rows) and YNT\_SSNQ (lower rows) CMAQ simulations during high ozone events A, B, and C. Wind directions are divided into 22.5 degree bins and the percentage of winds within each directional bin are indicated by the percentages on the wind rose plots. The colors within each wind direction bin indicate the distribution of observed and simulated ozone within 20ppbv bins as indicated by the color bars. The overall percentage of observed (OBS) and simulated (MOD) ozone within each ozone bin is indicated below the color bar for each site and simulation.

345

### 3.2.3 1-h ozone concentration and wind direction during high ozone events A, B, C

346

347

348

349

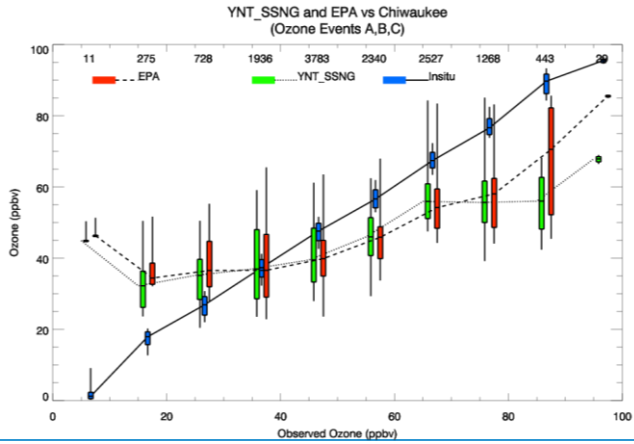
350

351

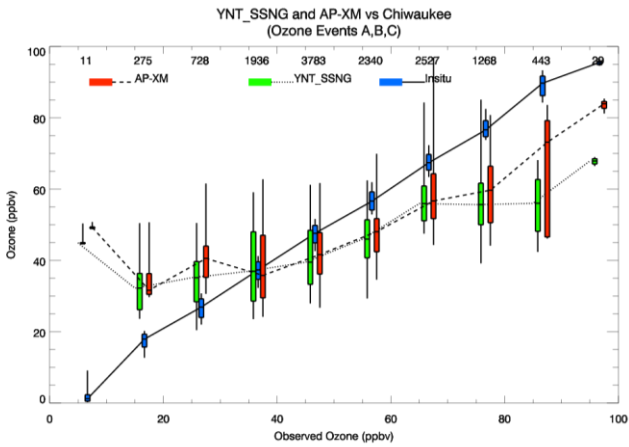
352

While the ozone wind roses presented above provide a n-overall comparison of the joint distribution of simulated and observed winds and ozone at these two stations, they do not provide a quantitative estimate of the errors in the simulations. In this section we have binned simulated and observed ozone and wind direction to provide a more quantitative characterization of the simulated biases. Figure 108 shows bar and whisker plots of 1.3km YNT\_SSNQ and AP\_XM\_obs/AP\_XMEPA CMAQ ozone simulations and 1-h averaged observed ozone at Chiwaukee Prairie and Sheboygan KA during high ozone events A, B, and C. Both simulations show systematic high biases for lower observed ozone concentrations (<math>< 40</math> ppbv) and low biases for higher ozone concentrations (> 50 ppbv) at both sites.

353 These results are consistent with the 8-hour maximum ozone biases for the 1.3km domain wide comparison (Figure  
 354 1). The [AP-XM-obs](#)/[AP-XM-EPA](#) simulation shows better agreement with observed ozone for the highest ozone (>85  
 355 ppbv) at both sites during high ozone events but shows a wider spread in the simulated distribution within each of  
 356 these high observed ozone bins at Chiwaukee Prairie. The [AP-XM-obs](#)/[AP-XM-EPA](#) and YNT\_SSNG CMAQ  
 357 simulations show similar distributions for observed ozone less than 80 ppbv.  
 358

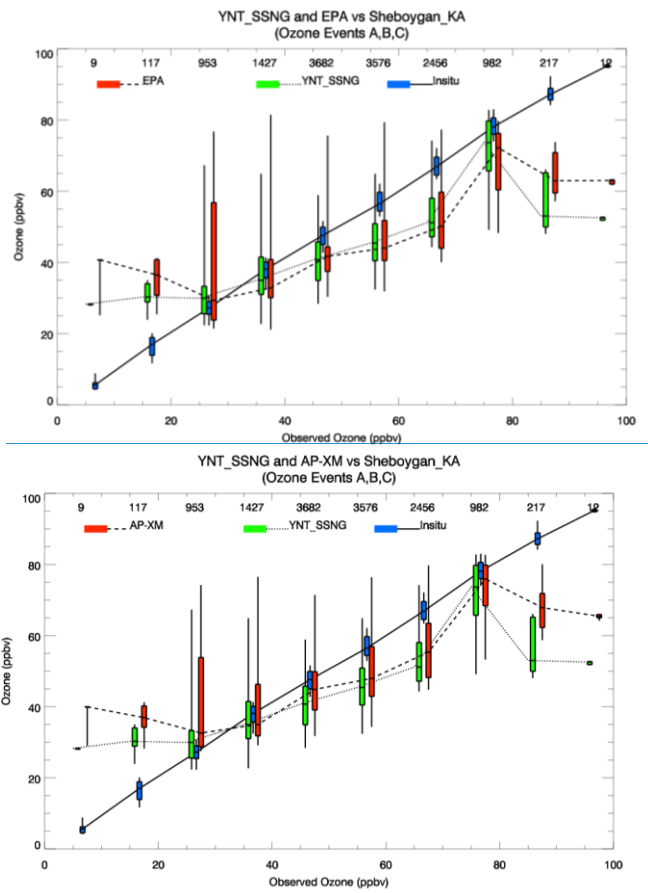


359



360





361

362

363

364

365

366

367

368

Figure 108. Bar and whisker plots showing the binned median ozone concentrations from the 1.3km AP-XM-obsAP-XMEPA (dashed) and YNT\_SSNG (dotted) CMAQ simulations and observed ozone (solid) at Chiwaukee Prairie (upper) and Sheboygan KA (lower) during high ozone events A, B, and C. The vertical bars show the 50% and the vertical lines show the 95% for the AP-XM-obsAP-XMEPA (red) and YNT\_SSNG (green) CMAQ simulations and observed ozone (blue). The total observed count within each 5 ppbv bin is indicated on the top of each panel.

369

370

371

372

373

374

375

376

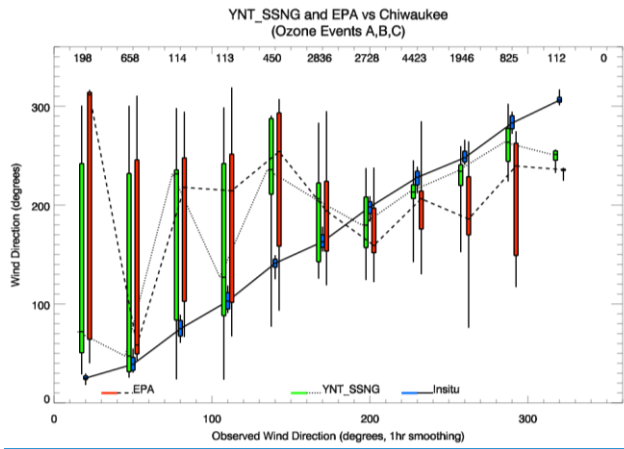
377

378

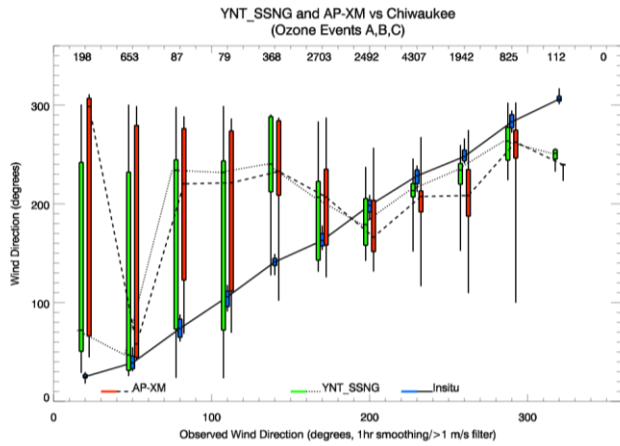
379

Figure 119 shows bar and whisker plots of 1.3km YNT\_SSNG and AP-XM-obsAP-XMEPA CMAQ wind direction simulations and 1-h averaged observed wind direction for wind-speeds greater than 1 m/s at Chiwaukee Prairie and Sheboygan KA during high ozone events A, B, and C. The 1 m/s threshold was included to reduce the impact of light and variable winds at these sites. Both simulations show a large westerly median bias and large variations and large variations in wind direction when the observed winds have an easterly component (0-180°) at Chiwaukee Prairie. This could be associated with errors in the timing of the arrival of the lake breeze, but a more detailed analysis along the lines of Wagner et al. (2022) would have to be performed to confirm this. Winds with an easterly component account for 30% of the observed wind directions at this site. Both simulations show a smaller systematic-easterly bias in median wind direction when the observed winds have a westerly component (180-360°) at Chiwaukee Prairie both sites, but the YNT\_SSNG simulation is in better agreement with observations during these periods, when the wind is from the southwest, west, and northwest (240-290°). The two simulations show small (~20°) easterly biases when the

380 observed winds are from the prevailing wind direction at Chiwaukee (south to west southwest, 180-260°) and  
 381 Sheboygan (south to south southwest, 180-220°) which account for 61% and 54% of the observed wind directions,  
 382 respectively. The YNT\_SSNNG simulation shows the smallest (~10°) easterly biases during prevailing winds at  
 383 Chiwaukee. The AP-XM simulation shows a small easterly biases when the observed winds have an easterly  
 384 component at Sheboygan KA while the YNT\_SSNNG simulation still shows some westerly biases in median wind  
 385 direction for these cases. Both simulations show somewhat larger easterly median biases when the observed winds  
 386 have a westerly component at Sheboygan KA, but the YNT\_SSNNG simulation is better agreement with observations  
 387 for these cases.  
 388



389  
 390



391  
 392

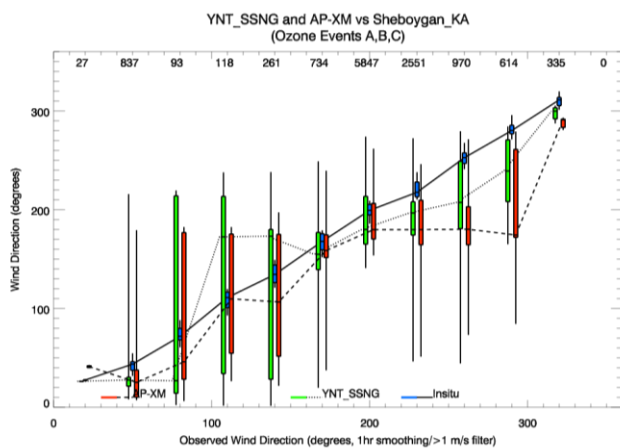
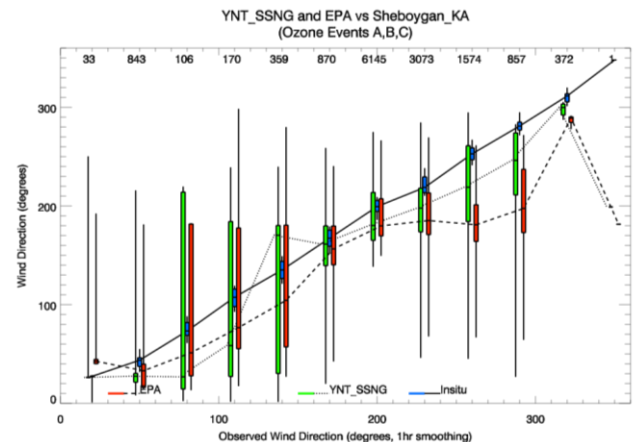


Figure 119. Bar and whisker plots showing the binned median wind direction from the 1.3km AP-XM-obsAP-XMEPA (dashed) and YNT\_SSNG (dotted) CMAQ simulations and observed wind direction (solid) at Chiwaukee Prairie (upper) and Sheboygan KA (lower) during high ozone events A, B, and C. The vertical bars show the 50% and the vertical lines show the 95% for the AP-XM-obsAP-XMEPA (red) and YNT\_SSNG (green) CMAQ simulations and 1-hour averaged observed wind direction (blue). The total observed count within each 20° bin is indicated on the top of the figures.

### 3.2.4 GEOTASO comparisons during high ozone events A, B, C

Here, we use GeoTASO (Nowlan et al., 2016) NO<sub>2</sub> and HCHO column measurements to verify ozone precursors within the YNT\_SSNG and AP-XM-obsAP-XMEPA simulations during high ozone events A, B, and C. Figure 120 shows the results of the NO<sub>2</sub> column analysis. Compared to observed NO<sub>2</sub> column measurements, the YNT\_SSNG and AP-XM-obsAP-XMEPA simulations have similar correlation (0.60 vs. 0.57) and the YNT\_SSNG has a substantially reduced bias (0.17 x 10<sup>15</sup> vs. 0.315 x 10<sup>15</sup> mol/cm<sup>2</sup>), although still within the uncertainty of the GeoTASO measurements. Figure 131 shows the results of the HCHO column analysis. Compared to observed HCHO column measurements, the YNT\_SSNG has a lower correlation than the AP-XM-obsAP-XMEPA simulation (0.24 vs. 0.334) and a larger bias (3.10 x 10<sup>15</sup> vs. 2.348 x 10<sup>15</sup> mol/cm<sup>2</sup>).

410  
 411 Nowlan et al. (2018) used comparisons between the GEOstationary Coastal and Air Pollution Events (GEO-CAPE)  
 412 Airborne Simulator (GCAS, which is similar to the GeoTASO instrument) NO<sub>2</sub> and HCHO retrievals and columns  
 413 estimated from airborne in-situ NO<sub>2</sub> and HCHO profiles to estimate mean precisions of  $1 \times 10^{15}$  mol/cm<sup>2</sup> and  $19 \times$   
 414  $10^{15}$  mol/cm<sup>2</sup> for the native (250m) resolution NO<sub>2</sub> and HCHO retrievals, respectively. The LMOS 2017 GeoTASO  
 415 radiances were co-added onto a 1km grid during the 2017 LMOS campaign so we anticipate that the precision of the  
 416 1km retrievals are better by a factor of 2. —Given the relatively high precision of GeoTASO NO<sub>2</sub> compared to the  
 417 column amounts observed during high ozone events A, B and C, we conclude that the high bias in NO<sub>2</sub> columns in  
 418 the ~~AP-XM\_obs~~AP-XM~~EPA~~ simulation is ~~significant, with more AP-XM NO<sub>2</sub> columns found outside the estimated~~  
 419  ~~$\pm 0.5 \times 10^{15}$  mol/cm<sup>2</sup> precision range then found in the YNT\_SSN simulation~~meaningful. We have less confidence  
 420 in the significance of the differences between the YNT\_SSN and ~~AP-XM\_obs~~AP-XM~~EPA~~ HCHO columns relative  
 421 to the GeoTASO retrievals since the observed HCHO columns are on the order of the precision of the instrument ( $10$   
 422  $\times 10^{15}$  mol/cm<sup>2</sup>) and the biases in the column HCHO ~~simulations measurements~~are both mostly less than the  
 423 GeoTASO precision during high ozone events A, B, and C. Overall, our results show the YNT\_SSN simulation  
 424 has an improved representation NO<sub>2</sub>, which is a primary ozone precursor, during these high ozone events.

Formatted: Subscript

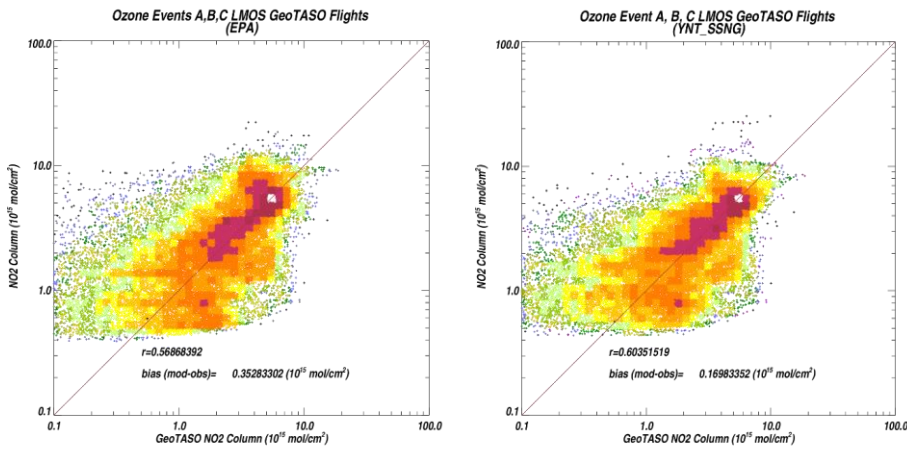
Formatted: Superscript

Formatted: Superscript

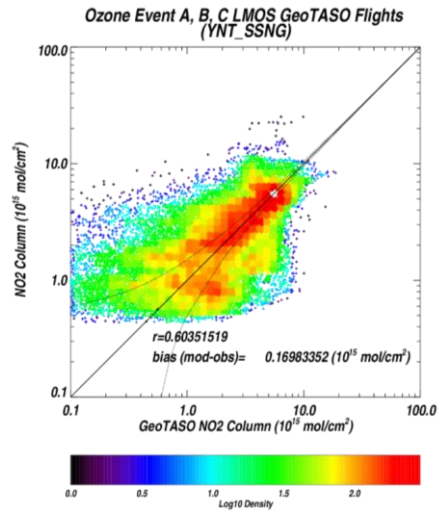
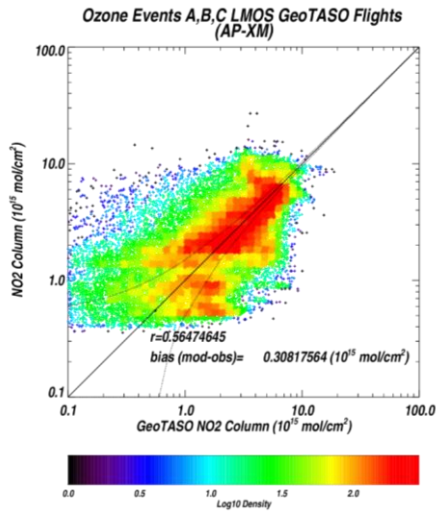
Formatted: Superscript

Formatted: Superscript

Formatted: Font: Bold



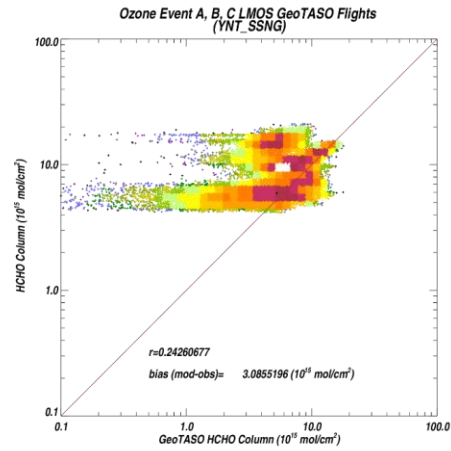
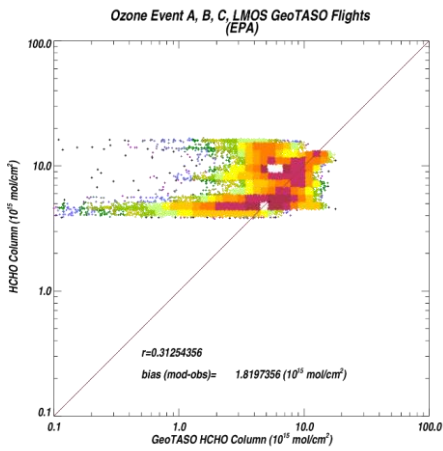
425  
 426



Formatted: Font: Bold

Figure 120. Scatter plots of 1.3km AP\_XM\_obs AP\_XM EPA (left) and YNT\_SSNG (right) NO<sub>2</sub> columns versus GEOTASO NO<sub>2</sub> columns ( $\times 10^{15}$  mol/cm<sup>2</sup>) during LMOS 2017 high ozone events A, B, and C. The dashed lines show the precision (+/-) of the GEOTASO NO<sub>2</sub> columns

Formatted: Subscript



427  
428  
429  
430  
431

432  
433

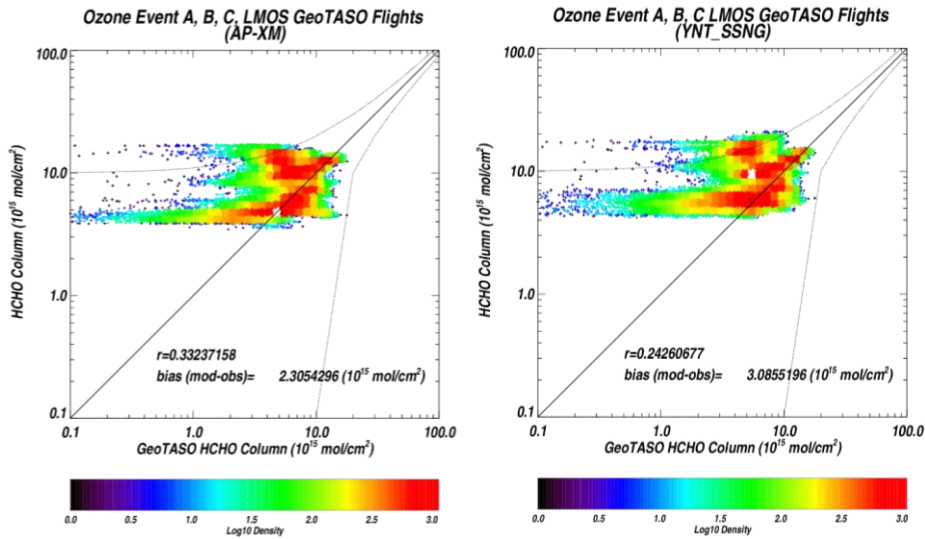


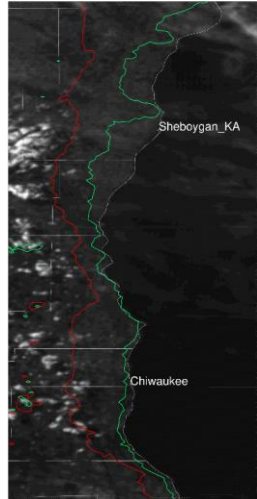
Figure 134. Same as in Figure 10 but for HCHO columns.

434  
435  
436

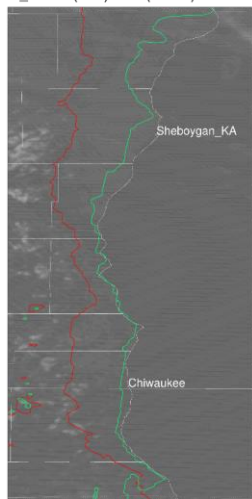
### 437 3.3 June 2, 2017 ozone exceedance event

438 The only ozone exceedance event that had significant inland penetration of the lake breeze at both Chiwaukee and  
 439 Sheboygan KA during LAMOS 2017 occurred on June 2<sup>nd</sup>, 2017 (Stanier et al, 2021; Wagner et al, 2022). —The  
 440 simulations on this day most clearly illustrate the differences between the ~~AP-XM\_obs~~AP-XMEPA and YNT\_SSNG  
 441 results. Figure 142 shows the observed visible (0.64 micron) reflectance from the Advanced Baseline Imager (ABI)  
 442 on the NOAA GOES-16 satellite and surface ozone concentrations from the YNT\_SSNG and ~~AP-XM\_obs~~AP-  
 443 XMEPA simulations, respectively, at 22 GMTUTC (5pm CDT) on June 2, 2017. To delineate the simulated  
 444 continental convective and stable maritime boundary layers we also show where the YNT\_SSNG and ~~AP-XM\_obs~~AP-  
 445 XMEPA simulated PBL heights are >1 km (Figure 142. Red or Green lines in the ABI panel). These contours roughly  
 446 correspond to the western most edge of the simulated marine boundary layer and indicate the extent of the penetration  
 447 of the lake breeze circulation. The ABI visible reflectances clearly show where the stable marine boundary layer  
 448 suppresses the formation of fair-weather cumulus clouds, which form within the turbulent continental boundary layer  
 449 and are evident to the west of the YNT\_SSNG 1-km PBL height contour. The YNT\_SSNG simulation shows a more  
 450 extensive penetration of high ozone concentrations inland, in agreement with the extent of the penetration of the  
 451 marine boundary layer. In contrast, the ~~AP-XM\_obs~~AP-XMEPA simulation shows very little penetration of the stable  
 452 marine boundary layer. This lake breeze penetration has a significant impact on the simulated surface ozone  
 453 distributions ~~with deeper penetration of high ozone inland. While the YNT\_SSNG simulation shows deeper~~  
 454 ~~penetration of the lake breeze circulation, it also leads to somewhat lower surface ozone concentrations near the~~  
 455 ~~shoreline leading to underestimates in the observed ozone concentrations at this time.~~

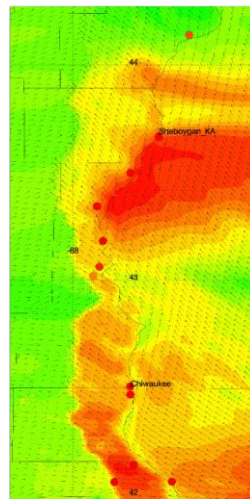
ABI Visible Reflectance June 02, 2017 22Z  
YNT\_SSSG (Red) AP-XM (Green) 1000m PBL



ABI Visible Reflectance June 02, 2017 22Z  
YNT\_SSSG (Red) EPA (Green) 1000m PBL

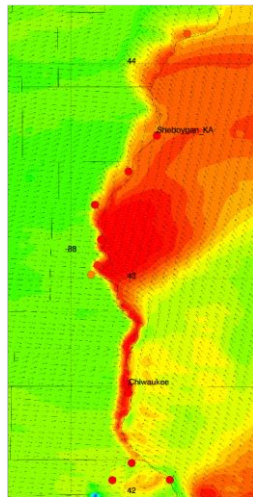


YNT\_SSSG  
06/02/2017 22Z

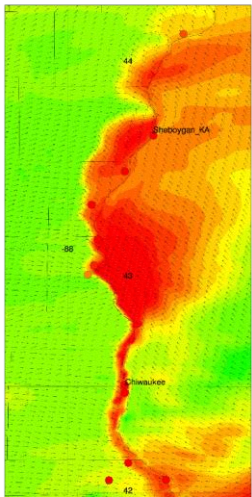


456

EPA  
06/02/2017 22Z



AP-XM  
06/02/2017 22Z



457

458

459

Figure 142: ABI visible (0.64micron) reflectance (left), YNT\_SSSG surface ozone (ppbv, middle), and ~~AP-XM-obs~~AP-XMEPA surface ozone (ppbv, right) at 22 GMTUTC on June 2, 2017. Observed AQS ozone concentrations at 22 GMTUTC

460 are shown as colored circles. Location of 1km YNT\_SSNG (Red) and ~~AP-XM\_obsAP-XM~~EPA (Green) PBL heights are  
461 also shown in the ABI (left) panel. The locations of the Shebogan, KA and Chiwaukee Prairie AQS monitors are labeled in  
462 each of the panels.  
463

464 Figure 153 shows comparisons between airborne GeoTASO, YNT\_SSNG, and ~~AP-XM\_obsAP-XM~~EPA column NO<sub>2</sub>  
465 along the western shore of Lake Michigan on June 2, 2017. Comparisons with column NO<sub>2</sub> distributions provide a  
466 means of comparing the fidelity of the lake breeze transport of ozone precursors during this high ozone event.  
467 Observed NO<sub>2</sub> columns peak near  $10 \times 10^{15}$  mol/cm<sup>2</sup> and shows penetration of the high NO<sub>2</sub> column amounts inland  
468 by the lake breeze circulation, consistent with the ABI visible reflectances. The observed NO<sub>2</sub> columns also show  
469 enhancements over the lake on the eastern part of the GeoTASO raster pattern that are best captured by the AP-XM  
470 simulation. The GeoTASO NO<sub>2</sub> columns show peak amounts of  $10 \times 10^{15}$  mol/cm<sup>2</sup> and significant inland penetration  
471 of higher NO<sub>2</sub> columns over the southern portion of the flight track. The YNT\_SSNG NO<sub>2</sub> column shows similar peak  
472 amounts and shows similar, but not as far inland, penetration of the high NO<sub>2</sub> columns. The ~~AP-XM\_obsAP-XM~~EPA  
473 NO<sub>2</sub> column shows localized NO<sub>2</sub> columns over  $15 \times 10^{15}$  mol/cm<sup>2</sup> along the Lake Michigan shoreline and does not  
474 predict as much onshore penetration. The narrow plume of higher GeoTASO NO<sub>2</sub> column extending to the northwest  
475 from the coast north of the Sheboygan KA AQS monitor is a signature of the Edgewater coal-fired power plant. The  
476 YNT\_SSNG and ~~AP-XM\_obsAP-XM~~EPA simulations also show this plume, but the YNT\_SSNG simulation does a  
477 better job of capturing the northwestward transport of the plume while the ~~AP-XM\_obsAP-XM~~EPA simulation shows  
478 transport of this narrow plume to the north-northeast.  
479

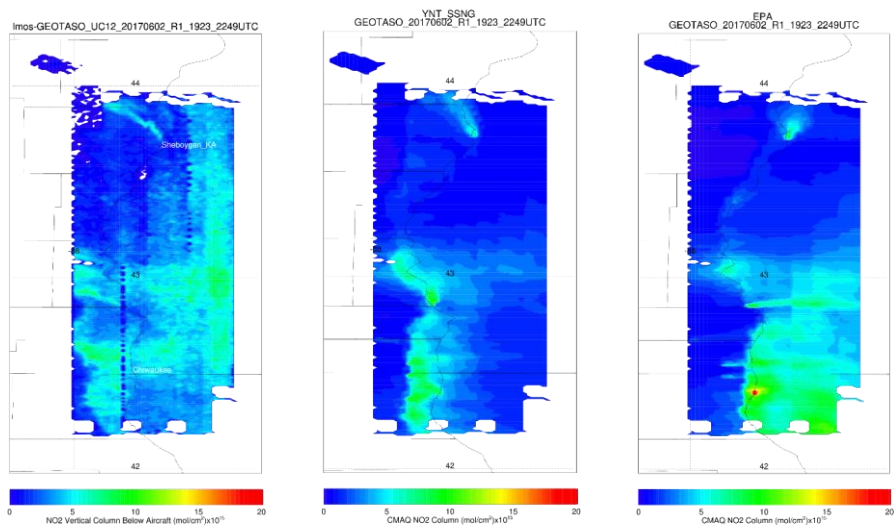
Formatted: Subscript

480 Figure 164 shows comparisons between airborne GeoTASO, YNT\_SSNG, and ~~AP-XM\_obsAP-XM~~EPA column  
481 HCHO along the western shore of Lake Michigan on June 2, 2017. HCHO columns vary much less spatially than NO<sub>2</sub>  
482 columns, ~~despite both anthropogenic and differing meteorologically driven biogenic VOC emissions influencing the~~  
483 ~~former, given that the former is formed through VOC oxidation~~ while the latter is primarily associated with  
484 anthropogenic emissions. Both simulations capture the observed north-to-south positive gradient providing some  
485 confidence in the larger scale gradients. However, the GeoTASO HCHO measurements show values in excess of  $10$   
486  $\times 10^{15}$  mol/cm<sup>2</sup> over Lake Michigan that are not captured in either the YNT\_SSNG or ~~AP-XM\_obsAP-XM~~EPA  
487 HCHO column simulations. Given the lower precision GeoTASO HCHO columns, the differences between the  
488 YNT\_SSNG and ~~AP-XM\_obsAP-XM~~EPA HCHO columns are difficult to quantify with these measurements. We  
489 note large differences between simulated and observed GeoTASO NO<sub>2</sub> and HCHO over the eastern portion of  
490 observations. These observations were collected later during the flight and therefore subject to larger uncertainties  
491 related to the impact of stratospheric NO<sub>2</sub> and ozone absorption interferences ~~resulting in a drift in the baseline~~  
492 ~~measurements.~~  
493

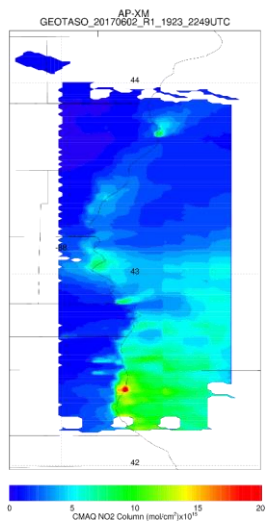
Formatted: Subscript

Formatted: Subscript



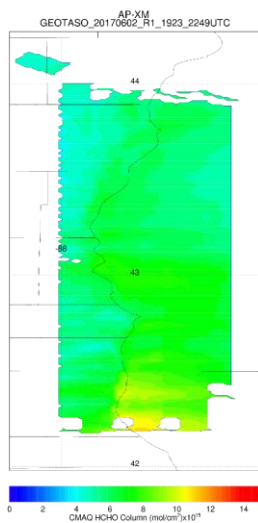
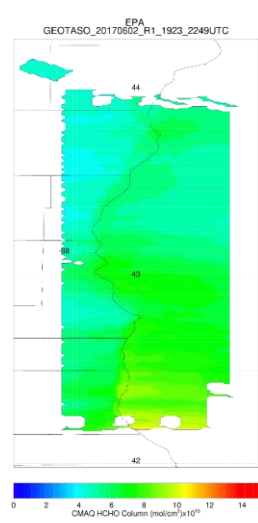
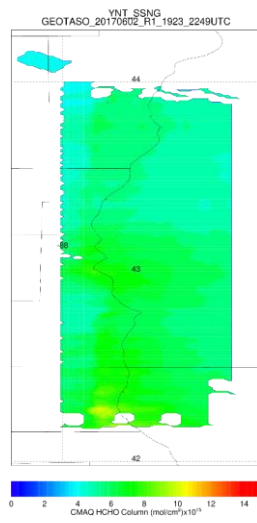
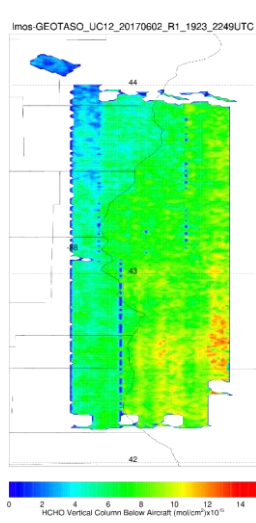


494



495  
496  
497

Figure 153: GEOTASO (left), YNT\_SSNG (middle), and AP-XM-obsAP-XMEPA (right) Column NO<sub>2</sub> ( $\times 10^{15}$  mol/cm<sup>2</sup>) on June 2, 2017. The location of the Sheboygan, KA AQS station is labeled in the GEOTASO column NO<sub>2</sub> panel.



498

499

500

501

Figure 16-4: GEOTASO (left), YNT\_SSG (middle), and AP-XM\_obsAP-XMEPA (right) Column HCHO ( $\times 10^{15}$  mol/cm<sup>2</sup>) on June 2, 2017.

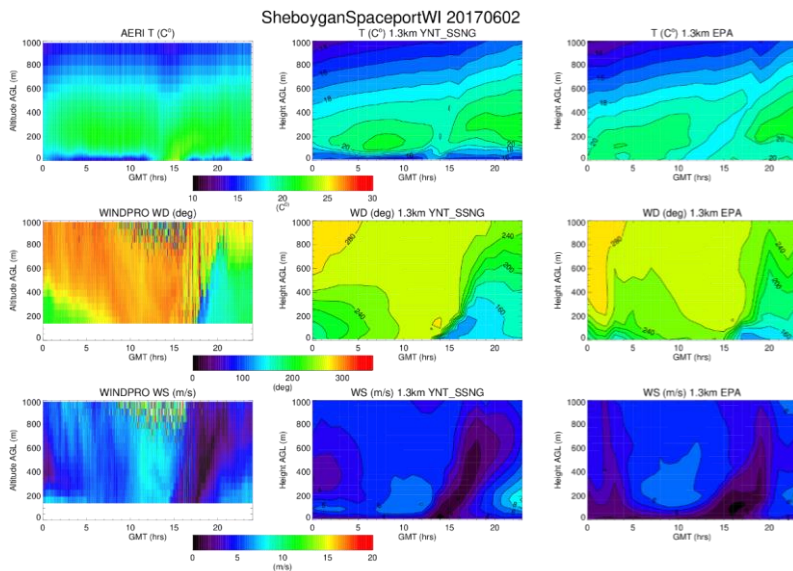
502  
503 Figure 175 shows comparisons between observed time height cross-sections of thermodynamic (temperature) and  
504 kinematic (wind) distributions at Sheboygan WI during the June 02, 2017 ozone exceedance event. Observed  
505 temperatures are obtained from the UW-Madison Atmospheric Emitted Radiance Interferometer (AERI) instrument  
506 (Knutson et al, 2004a,b) while wind direction and speed are obtained from a Halo Photonics doppler wind lidar  
507 instrument. Both of these instruments were deployed at the Sheboygan, WI ground site during LMOS 2017 (Stanier  
508 et al, 2021; Wagner et al, 2022). AERI temperatures show a well-defined nocturnal boundary layer with a thin layer  
509 of cold temperatures below 100-m AGL and a warmer layer extending up to approximately 600 m. The continental  
510 convective boundary layer begins to form as the sun rises (~12 GMTZ [7am CDT]). This is evident in the warmer  
511 surface temperatures near 15 GMTUTC (10am CDT). The AERI measurements show a new shallow layer of cooler  
512 air below 50m arriving at 17 GMTUTC (12pm CDT) associated with the stable marine boundary layer. Observed  
513 wind directions are out of the NW prior to 15 GMTUTC at 7m/s, rapidly diminish around 15 GMTUTC, and switch  
514 to the SE around 18 GMTUTC (1pm CDT) when the lake breeze reaches Sheboygan, WI. Both simulations show an  
515 easterly bias during the observed NW winds, which is consistent with the overall statistics during ozone events A, B,  
516 and C shown in Figure 11. The YNT\_SSN simulation captures the thermal structure of the nocturnal boundary layer  
517 (temperature differences are less than 2°C below 100 m) and timing of the arrival of the maritime boundary layer but  
518 underestimates the near surface (below 200 m) convective boundary layer surface temperatures by up to 10°C within  
519 the convective boundary layer at 15 GMT. The AP-XM simulation shows significant temperature differences are  
520 greater than 5°C below 100 m overestimates of the nocturnal boundary layer temperatures and shows a gradual  
521 warming of temperatures below 200 m after 15 GMT, resulting in large (greater than 7°C) overestimates in  
522 temperatures and no evidence of the cooler lake breeze. Both simulations underestimate the observed increase in wind  
523 speed prior to the arrival of the lake breeze by ~2 m/s. The YNT\_SSN simulation shows a more captures rapid shift  
524 in wind direction associated with the arrival of the lake breeze than the AP-XM simulation the vertical structure of the  
525 lake breeze wind speed and direction, but the timing of the switch in wind direction is about 3 hours too early in the  
526 YNT\_SSN simulation. This results in errors in wind speeds of up to 5 m/s near 200 m in the YNT\_SSN simulation  
527 prior to the observed reduction in wind speed at 15 GMT. The observed depth of the wind shift is underestimated in  
528 both simulations, but the YNT\_SSN simulation does a better job of capturing the vertical extent of the wind shift and  
529 reduction in wind speed above 200 m. This is most evident above 400 m where the AP-XM wind speeds are  
530 underestimated by up to 5 m/s. In contrast, the AP-XM\_obsEPA simulation shows no thermodynamic signature of a  
531 nocturnal or marine boundary layer and underestimates the sharp change in the observed windspeed and direction.

Formatted: Superscript

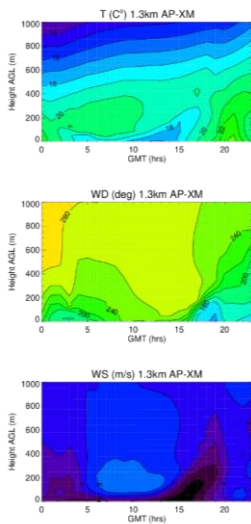
Formatted: Superscript

Formatted: Superscript

Formatted: Superscript



532

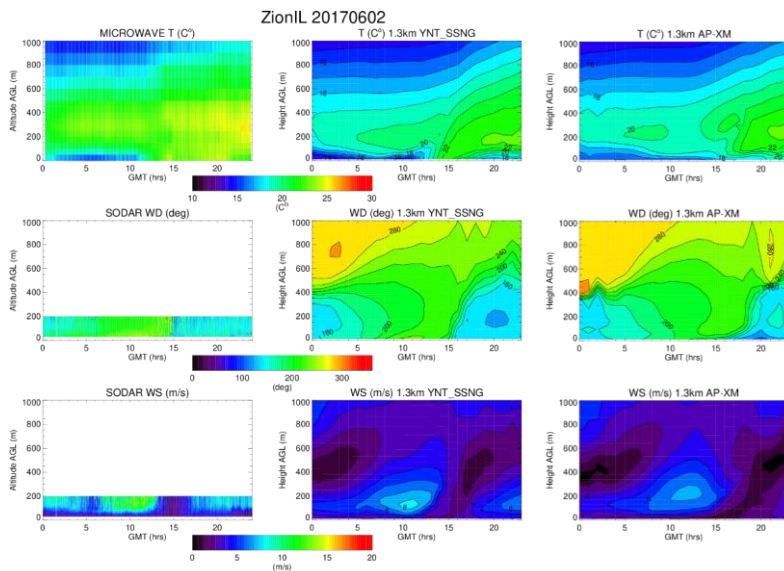


533  
534  
535  
536  
537  
538

Figure 17-5: Time height curtains of observed (left column), YNT\_SSNG (middle column), and ~~AP-XM\_obs~~AP-XMEPA (right column) temperature (T, C°, upper row), wind direction (WD, degrees, middle row), and wind speed (WS, m/s, lower row) at Sheboygan WI on June 2, 2017. Observed temperature is from UW-Madison AERI and observed winds are from the Halo Photonics doppler wind lidar instrument.

539 Figure 18 shows comparisons between observed time–height cross-sections of thermodynamic (temperature) and  
 540 kinematic (wind) distributions at Zion IL during the June 02, 2017 ozone exceedance event. Observed temperatures  
 541 are obtained from the Microwave Radiometer while wind direction and speed were observed using a Sound Detection  
 542 and Ranging (SODAR) instrument, both of which were provided by the University of Northern Iowa. Both of these  
 543 instruments were deployed at the Zion, IL ground site during LMOS 2017 (Stanier et al, 2021; Wagner et al, 2022).  
 544 Microwave temperatures show a well–defined nocturnal boundary layer with a thin layer of cooler temperatures below  
 545 100 m, similar to Sheboygan, WI (Figure 17) but not as cold. The continental convective boundary layer begins to  
 546 form as the sun rises (~12 GMT; ~7am CDT). This is evident in the warmer surface temperatures near 15 GMT  
 547 (10am CDT). In contrast to Sheboygan, the Microwave temperatures do not show a signature of the cooler air  
 548 associated with the stable marine boundary layer. This may be due to the fact that the Zion site is further inland than  
 549 the Sheboygan site and turbulent heat fluxes from the warmer land surface warm the marine layer. The Sodar  
 550 wind direction shows a sharp transition from south–westerly to south–easterly winds and a rapid reduction in  
 551 wind speed (from over 10 m/s to less than 5 m/s) at 15 GMT associated with the arrival of the lake breeze at the Zion site.  
 552 Both the YNT\_SSNNG and AP-XM simulations overestimate the temperature within the nocturnal boundary layer with  
 553 the AP-XM showing somewhat larger (>5°C) warm biases (>5°C) below 100 m compared to the YNT\_SSNNG (<5°C)  
 554 below 100m. The YNT\_SSNNG simulation captures the development of the continental convective boundary layer  
 555 better than the AP-XM simulation, which underestimates the observed temperatures by 5–7°C below 100 m between  
 556 sunrise (12 GMT) and 15 GMT (10am CDT). This cold bias persists until 20 GMT (3pm CDT) in the AP-XM  
 557 simulation. The YNT\_SSNNG simulation shows some evidence of a cooler lake breeze moving over the Zion site that  
 558 leads to a cold bias of 5–7°C at 20 GMT. The YNT\_SSNNG simulation does a very good job in capturing more accurately  
 559 captures the timing of the wind shift at 15 GMT, which is delayed by nearly 3 hours in the AP-XM simulation. Wind  
 560 speeds are similar in both simulations, although the YNT\_SSNNG simulation shows slightly higher (8 m/s versus 7  
 561 m/s) wind speeds prior to the arrival of the lake breeze and stronger (6 m/s versus 3 m/s) low level winds after 20  
 562 GMT, which are in better agreement with the SODAR measurements.

- Formatted: Superscript
- Formatted: Superscript
- Formatted: Superscript
- Commented [MH1]: switch UTC to Z to be consistent with other parts (or vice versa)
- Formatted: Superscript



563 Figure 18: Time height curtains of observed (left column), YNT\_SSNNG (middle column), and AP-XM (right column)  
 564 temperature (T, C°, upper row), wind direction (WD, degrees, middle row), and wind speed (WS, m/s, lower row) at Zion  
 565 IL on June 2, 2017. Observed temperatures were obtained using a Microwave Radiometer and observed winds are from a  
 566 SODAR instrument provided by Alan Czarnetski at the University of Northern Iowa.  
 567  
 568

569 **4. Discussion and Conclusions**

570 We have conducted an evaluation of two model simulations employing differing meteorological inputs, with the goal  
571 of identifying a model configuration best suited for characterizing the spatial and temporal variability of ozone and its  
572 precursors where lake breezes commonly affect local air quality along the Lake Michigan shoreline. We focus on the  
573 period of the LMOS campaign, 22 May – 22 June 2017, using the innermost grid of a triple-nested simulation around  
574 Lake Michigan, with a horizontal resolution of 1.3 km. The ~~AP-XM-obsAP-XMEPA~~ simulation used ~~the same~~  
575 ~~boundary layer and surface physics that are used within CMAQ best practice recommendations (Personal~~  
576 ~~communication, Jon Pleim and Robert Gilliam US EPA)~~ for WRF inputs ~~to the CMAQ model, including nudging to~~  
577 ~~observed near surface conditions~~; our YNT\_SSNG simulation used different WRF parameterizations, as well as  
578 constraints to satellite observations of green vegetation fraction and soil temperature and moisture, as detailed by  
579 Otkin et al. (2023).

580  
581 Both model simulations reasonably capture observed daily maximum 8-h average ozone amounts over the study  
582 period, however both simulations underestimate ~~ozone~~ ~~amounts~~ ~~at times with high ozone and overestimate~~  
583 ~~ozone when observed amounts were lower. These ozone biases are consistent with those simulated by Baker et~~  
584 ~~al. (2023).~~ Both model simulations also perform similarly on an hourly basis on high ozone days. We find the ~~AP-~~  
585 ~~XM-obsAP-XMEPA~~ simulation better represents hourly ozone when observed amounts are high (80-90 ppbv), and  
586 the YNT\_SSNG simulation overall biases are generally smaller (less negative) than those of the ~~AP-XM-obsAP-~~  
587 ~~XMEPA~~ simulation. Both simulations also tend to underestimate amounts of the ozone precursor HCHO, with smaller  
588 (less negative) biases in the YNT\_SSNG simulation. ~~This is inspite of the fact despite that the YNT\_SSNG uses a~~  
589 ~~more realistic, and lower (relative to climatology) Green Vegetation Fraction (which would tend to reduce biogenic~~  
590 ~~VOC emissions) suggesting that anthropogenic HCHO emissions may be playing a more important role in HCHO~~  
591 ~~concentrations in the YNT\_SSNG simulation. Both simulations significantly underestimate isoprene, with larger~~  
592 ~~(more negative) biases in the YNT\_SSNG simulation. This is also consistent with the use of more realistic, and lower~~  
593 ~~(relative to climatology) Green Vegetation Fraction in the YNT\_SSNG simulation. –likely resulting from the~~  
594 ~~incorporation of satellite derived GVF and therefore more realistic in line calculations of biogenic VOC emissions.~~  
595 We find the simulations are less similar in their representation of NO<sub>2</sub> amounts; while the ~~AP-XM-obsAP-XMEPA~~  
596 simulation tends to underestimate NO<sub>2</sub> at monitor sites, the YNT\_SSNG simulation has an overall high (positive) bias.

597  
598 Since the simulations use identical ~~anthropogenic~~ emissions and chemistry, the differences in modeled ozone and  
599 precursors are ~~linked to any~~ ~~the differences in biogenic emissions resulting from the input meteorology and from~~  
600 ~~differences in boundary layer mixing, both~~ horizontal and vertical transport. ~~In modeling the same time period, Baker~~  
601 ~~et al. (2023)~~ In Part I of this study, Otkin et al. (2022) noted the ~~AP-XM-obsAP-XMEPA~~ simulation had an overall  
602 low bias in wind speed, the YNT\_SSNG simulation had a positive bias, and the simulations had similar RMSE. Here,  
603 we find many similarities between simulations on high ozone days. At Chiwaukee Prairie, we find both simulations  
604 capture the highest ozone amounts transported from the SSE. On high ozone days at Sheboygan KA, observed winds  
605 tend to be SSW, while both models show highest ozone amounts transported from the SSE. At ~~Chiwaukee Prairie~~  
606 ~~both~~ ~~locations~~, both simulations tend to have a westerly bias when observed winds have an easterly (onshore) component.

607  
608 We find greater differences in column amounts of ozone precursors. The ~~AP-XM-obsAP-XMEPA~~ simulation has a  
609 negative bias in near-surface NO<sub>2</sub> ~~at Sheboygan, a high bias in near-surface NO<sub>2</sub> at Zion,~~ a positive bias in column  
610 NO<sub>2</sub> amounts, and elevated column amounts concentrated along the Lake Michigan shoreline during the ozone  
611 exceedance event on June 2<sup>nd</sup>. The YNT\_SSNG simulation has a small positive bias in NO<sub>2</sub> column amounts, with  
612 elevated column amounts extending further inland on the lake-breeze enhanced ozone event on June 2<sup>nd</sup>. While these  
613 differences reflect the parameterizations used to generate input meteorology, differences in vertical mixing, and  
614 ensuing column amounts of NO<sub>2</sub> and HCHO discussed here, ~~they~~ are further complicated by CMAQ using the ACM2  
615 parameterization for vertical diffusion—a mismatch for the YNT\_SSNG simulation that influences our evaluation  
616 since it leads to differences in boundary layer mixing. Still, the NO<sub>2</sub> column comparisons provide support for the  
617 improved representation of lake breeze transport of ozone precursors in the YNT\_SSNG simulation. Future model  
618 comparisons with upcoming geostationary observations will allow for maturing analysis for assessing model  
619 performance with respect to the diurnal evolution of precursors during ozone events.

620  
621 Our thermodynamic and kinematic comparison of the ~~AP-XM-obsAP-XMEPA~~ and YNT\_SSNG simulations show  
622 improved representation of not only the extent, but of the timing of the lake breeze in the YNT\_SSNG simulation ~~at~~  
623 ~~Sheboygan, WI and Zion, IL for the June 2, 2017 ozone episode.~~ This is consistent with the meteorological analysis

Formatted: Subscript

624 presented in Part 1 of this study, where the YNT\_SSNG had a better representation of diurnal patterns (Otkin et al.,  
625 2023<sup>2</sup>). However, we note that the meteorological inputs to our CMAQ simulations are hourly, as is typically used in  
626 air quality modeling studies. Both simulations would likely benefit from sub-hourly winds given the rapid changes  
627 that can occur in the presence of lake and land breeze circulations. For this, a more tightly a-two-way-coupled model  
628 such as WRF-CMAQ (Wang et al., 2021) would be better suited for a goal of better simulating the fine temporal and  
629 spatial scales of lake breeze transport and chemistry.

630  
631 This analysis complements other studies in evaluating the impact of changing meteorological inputs and  
632 parameterizations on air quality in a complex environment. Appel et al. (2014) also found improved representation of  
633 ozone in environments with bay and sea breezes with the addition of high-resolution SST into the WRF and CMAQ  
634 modeling framework. Cheng et al. (2012) underscored the importance of PBL parameterization in simulating land-sea  
635 breezes and their impacts on near-surface ozone. Similar to our work, Banks and Baldasano (2016) evaluated the  
636 impacts of PBL parameterizations on air quality and also found ambiguous results, with the simulation using the YSU  
637 PBL better capturing observed NO<sub>2</sub>, and the simulation using the ACM2 PBL better capturing observed ozone. Future  
638 work will be able to take advantage of ongoing improvements to both WRF and CMAQ, such as an update to the  
639 calculation of vegetative fraction and PX-LSM soil parameters in WRF (Appel et al., 2021), and should explore the  
640 relationships among spatial and temporal resolution of meteorological parameterizations themselves along with those  
641 of the modeling framework.

#### 642 Acknowledgments

643 Funding for this project was provided by the NASA Health and Air Quality (HAQ) program via grant  
644 #80NSSC18K1593. We wish to thank the 2017 Lake Michigan Ozone Study Instrument teams for the GeoTASO,  
645 AERI, Doppler Wind Lidar, Microwave SODARedax, and surface measurements used in this study. We also wish to  
646 thank Laura Judd and Scott Janz for their review of the manuscript.

#### 647 References

- 648  
649  
650  
651 Abdi-Oskouei, M., G-Carmichael, G. M-Christiansen, M., G-Ferrada, G., B-Roozitalab, B., N-Sobhani, N., K-  
652 Wade, K., A-Czarnetzki, A., R-B-Pierce, R. B., T-Wagner, T., and C-Stanier, C. (2020); Sensitivity of  
653 Meteorological Skill to Selection of WRF-Chem Physical Parameterizations and Impact on Ozone Prediction  
654 During the Lake Michigan Ozone Study (LMOS), J. Geophys. Res. Atmos., 125(5),  
655 doi:10.1029/2019JD031971, 2020.
- 656 Adams, E. (2020); 2017 v1 NEI Emissions Modeling Platform (Premerged CMAQ-ready Emissions),  
657 doi:10.15139/S3/TCR6BB, UNC Dataverse, V1, 2020.
- 658 Adelman, Z. (2020); LADCO public issues, <https://www.ladco.org/public-issues/>, 2020.
- 659 Appel, K. W., R-C-Gilliam, R. C., J-E-Pleim, J. E., G-Pouliot, G., D-C-Wong, D. C., S-J-Roselle, S. J., and R-  
660 Mathur, R. (2014); Improvements to the WRF-CMAQ modeling system for fine-scale air quality applications  
661 to the DISCOVER-AQ Baltimore/Washington D.C. campaign. EM: Air and Waste Management Associations  
662 Magazine for Environmental Managers. Air & Waste Management Association, September 2014 Issue, 16-21,  
663 2014.
- 664 Appel, K. W., Napelenok, S. L., Foley, K. M., Pye, H. O. T., Hogrefe, C., Leucken, D. J., Bash, J. O., Roselle, S. J.,  
665 Pleim, J. E., Foroutan, H., Hutzell, W. T., Pouliot, G. A., Sarwar, G., Fahey, K. M., Gantt, B., Gilliam, R. C.,  
666 Heath, N. K., Kang, D., Mathur, R., Schwede, D. B., Spero, T. L., Wong, D. C., and Young, J. O.: Description  
667 and evaluation of the Community Multiscale Air Quality (CMAQ) modeling system version 5.1, Geosci.  
668 Model Dev., 10, 1703-1732, doi:10.5194/gmd-10-1703-2017, 2017.
- 669 Appel, K. W., J-O-Bash, J. O., K-M-Fahey, K. M., K-M-Foley, K. M., R-C-Gilliam, R. C., E-Hogrefe, C., W-T-  
670 Hutzell, W. T., D-Kang, D., R-Mathur, R., B-N-Murphy, B. N., S-L-Napelenok, S. L., C-G-Nolte, C. G.,  
671 J-E-Pleim, J. E., G-A-Pouliot, G. A., H-O-T-Pye, H. O. T., L-Ran, L., S-J-Roselle, S. J., G-Sarwar, G., D-  
672 B-Schwede, D. B., F-I-Sidi, F. I., T-L-Spero, T. L., and D-C-Wong, D. C.; (2021), The Community  
673 Multiscale Air Quality (CMAQ) model versions 5.3 and 5.3.1: system updates and evaluation, Geosci. Model  
674 Dev., 14, 2867-2897, doi: 10.5194/gmd-14-2867-2021, 2021.
- 675 Baker, K., Liljegren, J., Valin, L., Judd, L., Szykman, J., Millet, D. B., Czarnetzki, A., Whitehill, A., Murphy, B.,  
676 Stanier, C.: Photochemical model representation of ozone and precursors during the 2017 Lake Michigan  
677 ozone study (LMOS), Atmos. Environ., 293, 119465, doi:10.1016/j.atmosenv.2022.119465, 2023.
- 678 Banks, B. F., and J-M-Baldasano, J. M. (2016); Impact of WRF model PBL schemes on air quality simulations  
679 over Catalonia, Spain, Sci. Total Environ., 572, 98-113, doi: 10.1016/j.scitotenv.2016.07.167, 2016.

Formatted: Font: Not Italic

Formatted: Font: Not Italic

Formatted: Font: Not Italic

Formatted: Font: Not Italic

580 Brook, J. R., Makar, P. A., Sills, D. M. L., Hayden, K. L., and McLaren, R.: Exploring the nature of air quality over  
581 southwestern Ontario: main findings from the Border Air Quality and Meteorology Study, *Atmos. Chem.*  
582 *Phys.*, 13(20), 10461-10482, doi:10.5194/acp-13-10461-2013, 2013.

583 Byun, D., and ~~K. L. Schere, K. L. (2006)~~, Review of the governing equations, computational algorithms, and other  
584 components of the Models-3 Community Multiscale Air Quality (CMAQ) modeling, *Appl. Mech. Rev.*, 59(1-  
585 6), 51-77, doi:10.1115/1.2128636, 2006.

586 Carlton, A. G., and ~~K. R. Baker, K. R. (2014)~~, Photochemical modeling of the Ozark isoprene volcano: MEGAN,  
587 BEIS, and their impacts on air quality predictions, *Environ. Sci. Technol.*, 45(10), 4438-45,  
588 doi:10.1021/es200050x, 2011.

589 Case, J. L. ~~(2016)~~, From drought to flooding in less than a week over South Carolina, *Results Phys.*, 6, 1183-1184,  
590 doi:10.1016/j.rinp.2016.11.012, 2016.

591 Case, J. L., and ~~B. T. Zavodsky, B. T. (2018)~~, Evolution of drought in the southeastern United States from a land  
592 surface modeling perspective, *Results Phys.*, 8, 654-656, doi:10.1016/j.rinp.2017.12.029, 2018.

593 Chen, F., and ~~J. Dudhia, J. (2004)~~, Coupling an advanced land-surface/hydrology model with the Penn State/NCAR  
594 MM5 modeling system. Part I: Model description and implementation, *Mon. Wea. Rev.*, 129(4), 569-585,  
595 doi:10.1175/1520-0493(2001)129<0569:CAALSH>2.0.CO;2, 2001.

596 Cheng, F.-Y., ~~S.-C. Chin, S.-C.~~, and ~~T.-H. Liu, T.-H. (2012)~~, The role of boundary layer schemes in  
597 meteorological and air quality simulations of the Taiwan area, *Atmos. Env.*, 54, 714-727, doi:  
598 10.1016/j.atmosenv.2012.01.029, 2012.

599 Cleary, P. A., ~~A. Dickens, A. M. McIlquham, M. M. Sanchez, M. K. Geib, K. C. Hedberg, C. J. Hupy, J. M. W.~~  
700 ~~Watson, M. W. M. Fuoco, M. E. R. Olson, E. R. R. B. Pierce, R. B. C. Stanier, C. R. Long, R. L. Valin, L.~~  
701 ~~S. Conley, S. and M. Smith, M. (2021)~~, Impacts of lake breeze meteorology on ozone gradient observations  
702 along Lake Michigan shorelines in Wisconsin, *Atmos. Env.*, 269, 118834, 2021,  
703 doi:10.1016/j.atmosenv.2021.118834, 2021.

704 Clifton, O. E., ~~D. L. Lombardo, D. L. A. M. Fiore, A. M. F. Paulot, F. and L. W. Horowitz, L. W. (2020)~~,  
705 Stomatal conductance influences interannual variability and long-term changes in regional cumulative plant  
706 uptake of ozone, *Env. Res. Lett.*, 15(11), 114059, doi:10.1088/1748-9326/abc3f1, 2020.

707 Daggett, D. A., ~~J. D. Myers, J. D. and H. A. Anderson, H. A. (2000)~~, Ozone and particulate matter air pollution in  
708 Wisconsin: trends and estimates of health effects, *Wis. Med. J.*, 99(8), 47-51, 2000.

709 Di, Q., ~~Y. Wang, Y. A. Zanobetti, A. Y. Wang, Y. P. Koutrakis, P. C. Choirat, C. F. Dominici, F. and J. D.~~  
710 ~~Schwartz, J. D. (2017)~~, Air Pollution and Mortality in the Medicare Population, *N. Engl. J. Med.*, 376, 2513-  
711 2522, doi:10.1056/NEJMoa1702747, 2017.

712 Dye, T. S., ~~P. T. Roberts, P. T. and M. E. Koc, M. E. (1995)~~, M. E.: Observations of Transport Processes for Ozone and  
713 Ozone Precursors during the 1991 Lake Michigan Ozone Study, *J. Appl. Meteorol. Climatol.*, 34(8), 1877-  
714 1889, doi:10.1175/1520-0450(1995)034<1877:OOTPFO>2.0.CO;2, 1995.

715 Ek, M. B., ~~K. E. Mitchell, K. E. Y. Lin, Y. E. Rogers, E. P. Grunmann, P. V. Koren, V. G. Gayno, G. and J. D.~~  
716 ~~Tarpley (2003)~~, J. D.: Implementation of Noah land surface model advances in the National Centers for  
717 Environmental Prediction operational mesoscale Eta model, *J. Geophys. Res.*, 108(D22), 8851,  
718 doi:10.1029/2002JD003296, 2003.

719 Emery, C., ~~J. Jung, J. B. Koo, B. and G. Yarwood, G. (2015)~~, Improvements to CAMx Snow Cover Treatments  
720 and Carbon Bond Chemical Mechanism for Winter Ozone. Final Report, prepared for Utah Department of  
721 Environmental Quality, prepared by Ramboll Environ, Novato, CA, 2015.

722 Fast, J. D., and ~~W. E. Heilman, W. E. (2003)~~, The Effect of Lake Temperatures and Emissions on Ozone Exposure  
723 in the Western Great Lakes Region, *J. Appl. Meteorol. Climatol.*, 42(9), 1197-1217, doi:10.1175/1520-  
724 0450(2003)042<1197:TEOLTA>2.0.CO;2, 2003.

725 Foley, T., ~~E. A. Betterton, E. A. P. E. R. Jacko, P. E. R. and J. Hillery, J. (2011)~~, Lake Michigan air quality: The  
726 1994-2003 LADCO Aircraft Project (LAP), *Atmos. Env.*, 45(18), 3192-3202,  
727 doi:10.1016/j.atmosenv.2011.02.033, 2011.

728 Gilliam, R. C., and ~~J. E. Pleim, J. E. (2010)~~, Performance assessment of new land surface and planetary boundary  
729 layer physics in the WRF-ARW, *J. Appl. Meteorol. Climatol.*, 49(4), 760-774, doi:  
730 10.1175/2009JAMC2126.1, 2010.

731 Guenther, A., ~~C. N. Hewitt, C. N. D. Erickson, D. R. Fall, R. C. Geron, C. T. Graedel, T. P. Harley, P. L.~~  
732 ~~Klinger, L. M. Lerdau, M. W. A. McKay, W. A. T. Pierce, T. B. Scholes, B. R. Steinbrecher, R. R.~~  
733 ~~Tallamraju, R. J. Taylor, J. and P. Zimmerman, P. (1995)~~, A global model of natural volatile organic  
734 compound emissions, *J. Geophys. Res.*, 100(D5), 8873-8892, doi: 10.1029/94JD02950, 1995.

Formatted: Font: Not Italic

Formatted: Font: Not Italic

Formatted: Font: Not Italic

Formatted: Font: Not Italic

Formatted: Font: Not Italic

Formatted: Font: Not Italic

Formatted: Font: Not Italic

Formatted: Font: Not Italic

Formatted: Font: Not Italic

Formatted: Font: Not Italic

Formatted: Font: Not Italic

Formatted: Font: Not Italic

Formatted: Font: Not Italic

Formatted: Font: Not Italic

Formatted: Font: Not Italic

Formatted: Font: Not Italic

Formatted: Font: Not Italic

Formatted: Font: Not Italic

Formatted: Font: Not Italic



735 Hall, S. J., ~~P. A. Matson, P. A., and P. M. Roth, P. M.:~~ (1996), NOx emissions from soil: Implications for air quality  
736 modeling in agricultural regions, *Annu. Rev. Energy Environ.*, 21(1), 311-346, doi:  
737 10.1146/annurev.energy.21.1.311, 1996.

738 He, C., ~~J. Cheng, J., X. Zhang, X., M. Douthwaite, M., S. Pattison, S., and Z. P. Hao (2019), Z. P.:~~ Recent  
739 advances in the catalytic oxidation of volatile organic compounds: A review based on pollutant sorts and  
740 sources, *Chem. Rev.*, 119(7), 4471-4568, doi:10.1021/acs.chemrev.8b00408, 2019.

741 ~~He, H., Tarasick, D. W., Hocking, W. K., Carey-Smith, T. K., Rochon, Y., Zhang, J., Makar, P. A., Osman, M.,~~  
742 ~~Brook, J., Moran, M. D., Jones, D. B. A., Mihele, C., Wei, J. C., Osterman, G., Argall, P. S., McConnell, J.,~~  
743 ~~and Bourqui, M. S.:~~ Transport analysis of ozone enhancement in Southern Ontario during BAQS-Met, *Atmos.*  
744 *Chem. Phys.*, 11(6), 2569-2583, doi:10.5194/acp-11-2569-2011, 2011.

745

746 Hong, S.-Y., ~~Y. Noh, Y., and J. Dudhia, J.:~~ (2006), A new vertical diffusion package with explicit treatment of  
747 entrainment processes, *Mon. Wea. Rev.*, 134(9), 2318-2341, doi:10.1175/MWR3199.1, 2006.

748 Iacono, M. J., ~~J. S. Delamere, J. S., E. J. Mlawer, E. J., M. W. Shephard, M. W., S. A. Clough, S. A., and W. D.~~  
749 ~~Collins, W. D.:~~ (2008), Radiative forcing by long-lived greenhouse gases: Calculations with the AER radiative  
750 transfer models, *J. Geophys. Res.*, 113(D13), doi:10.1029/2008JD009944, 2008.

751 Judd, L. A., ~~J. A. Al-Saadi, J. A., S. J. Janz, S. J., M. G. Kowalewski, M. G., R. B. Pierce, R. B., J. J. Szykman, J.~~  
752 ~~J., L. C. Valin, L. C., R. Swap, R., A. Cede, A., M. Mueller, M., M. Tidfengraber, M., N. Abuhassan, N., and~~  
753 ~~D. Williams (2019), D.:~~ Evaluating the impact of spatial resolution on tropospheric NO2 column  
754 comparisons within urban areas using high-resolution airborne data, *Atmos. Meas. Tech.*, 12(11), 6091-6111,  
755 doi: 10.5194/amt-12-6091-2019, 2019.

756 Juncosa Calahorrano, J. F., ~~J. Lindaas, J., K. O'Dell, K., B. B. Palm, B. B., Q. Peng, Q., F. Flocke, F., I. B. Pollack,~~  
757 ~~I. B., L. A. Garofalo, L. A., D. K. Farmer, D. K., J. R. Pierce, J. R., J. L. Collett Jr., J. L., A. Weinheimer, A.,~~  
758 ~~T. Campos, T., R. S. Hornbrook, R. S., S. R. Hall, S. R., K. Ullmann, K., M. A. Pothier, M. A., E. C. Apel, E.~~  
759 ~~C., W. Permar, W., L. Hu, L., A. J. Hills, A. J., D. Montzka, D., G. Tyndall, G., J. A. Thornton, J. A., and E.~~  
760 ~~V. Fischer (2020), E. V.:~~ Daytime oxidized reactive nitrogen partitioning in Western U.S. wildfire smoke  
761 plumes, *J. Geophys. Res. Atmos.*, 126(4), doi:10.1029/2020JD033484, 2020.

762 Kain, J. S.: (2004), The Kain-Fritsch convective parameterization: An update, *J. Appl. Meteorol. Climatol.*, 43(1),  
763 170-181, doi:10.1175/1520-0450(2004)043<0170:TKCPAU>2.0.CO;2, 2004.

764 Knuteson, R. O., ~~and Coauthors, 2004a:~~ Revercomb, H. E., Best, F. A., Ciganovich, N. C., Dedecker, R. G., Dirks, T. P.,  
765 Ellington, S. C., Feltz, W. F., Garcia, R. K., Howell, H. B., Smith, W. L., Short, J. F., and Tobin D. C.,  
766 2004a: Atmospheric emitted radiance interferometer. Part I: Instrument design. *J. Atmos. Oceanic Technol.*,  
767 21, 1763-1776, <https://doi.org/10.1175/JTECH-1662.1>, 2004a.

768 Knuteson, R. O., ~~and Coauthors, 2004b:~~ Revercomb, H. E., Best, F. A., Ciganovich, N. C., Dedecker, R. G., Dirks,  
769 T. P., Ellington, S. C., Feltz, W. F., Garcia, R. K., Howell, H. B., Smith, W. L., Short, J. F., and Tobin D. C.,  
770 Atmospheric emitted radiance interferometer. Part II: Instrument performance. *J. Atmos. Oceanic Technol.*,  
771 21, 1777-1789, <https://doi.org/10.1175/JTECH-1663.1>, 2004b.

772 Lamsal, L. N., ~~R. V. Martin, R. V., A. van Donkelaar, A., E. A. Celarier, E. A., E. J. Bucsela, E. J., K. F. Boersma,~~  
773 ~~K. F., R. Dirksen, R., C. Luo, C., and Y. Wang (2010), Y.:~~ Indirect validation of tropospheric nitrogen  
774 dioxide retrieved from the OMI satellite instrument: Insight into the seasonal variation of nitrogen oxides at  
775 northern midlatitudes, *J. Geophys. Res. Atmos.*, 115(D5), doi:10.1029/2009JD013351, 2010.

776 Lawrence, M. G., and ~~P. J. Crutzen (1999), P. J.:~~ Influence of NOx emissions from ships on tropospheric  
777 photochemistry and climate, *Nature*, 402, 167-170, doi: 10.1038/46013, 1999.

778 Lee, D., Wang, J., Jiang, X., Lee, Y., Jang, K.: Comparison between atmospheric chemistry model and observations  
779 utilizing the RAQMS-CMAQ linkage, *Atmospheric Environment*, doi: 10.1016/j.atmosenv.2012.06.083,  
780 2012.

781 Leitch, J. W., ~~T. Delker, T., W. Good, W., L. Ruppert, L., F. Murcray, F., K. Chance, K., X. Liu, X., C. Nowlan, C.,~~  
782 ~~S. Janz, S., N. A. Krotkov, N. A., K. E. Pickering, K. E., M. Kowalewski, M., and J. Wang, J.:~~ (2014), The  
783 GeoTASO airborne spectrometer project, *Proc. SPIE* 9218, Earth Observing Systems XIX, 17-21 August  
784 2014, San Diego, doi: 10.1117/12.2063763, 2014.

785 Lelieveld, J., ~~J. S. Evans, J. S., M. Fnais, M., D. Giannadaki, D., and A. Pozzer, A.:~~ (2015), The contribution of  
786 outdoor air pollution to premature mortality on the global scale, *Nature*, 525(7569), 367-371,  
787 doi:10.1038/nature15371, 2015.

788 Lennartson, G. J., and ~~M. D. Schwartz (2002), M. D.:~~ The lake breeze-ground-level ozone connection in eastern  
789 Wisconsin: a climatological perspective, *Int. J. Climatol.*, 22(11), 1347-1364, doi:10.1002/joc.802, 2002.

Formatted: Font: Not Italic

Formatted: Font: Not Italic

Formatted: Font: Not Italic

Formatted: Font: Not Italic

Formatted: Font: Not Italic

Formatted: Font: Not Italic

Formatted: Font: Not Italic

Formatted: Font: Not Italic

Formatted: Font: Not Italic

Formatted: Font: Not Italic

Formatted: Font: Not Italic

Formatted: Font: Not Italic

790 Luecken, D. J., ~~G.~~ Yarwood, ~~G.~~, and ~~W. T.~~ Hutzell, ~~W. T.~~: (2019), Multipollutant modeling of ozone, reactive  
791 nitrogen and HAPs across the continental US with CMAQ-CB6, *Atmos. Environ.*, 201(July), 62–72,  
792 doi:10.1016/j.atmosenv.2018.11.060, 2019.

793 ~~Makar, P. A., Zhang, J., Gong, W., Stroud, C., Sills, D., Hayden, K. L., Brook, J., Levy, I., Mihele, C., Moran, M.,~~  
794 ~~D., Tarasick, D. W., He, H., and Plummer, D.: Mass tracking for chemical analysis: the causes of ozone~~  
795 ~~formation in southern Ontario during BAQS-Met 2007, *Atmos. Chem. Phys.*, 10(22), 11151–11173,~~  
796 ~~doi:10.5194/acp-10-11151-2010, 2010.~~

797 Manisalidis, I., ~~E.~~ Stavropoulou, ~~E.~~, ~~A.~~ Stavropoulos, ~~A.~~, and ~~E.~~ Bezirtzoglou, ~~E.~~: (2020), Environmental and Health  
798 Impacts of Air Pollution: A Review, *Front. Public Health*, 8(14), doi: 10.3389/fpubh.2020.00014, 2020.

799 Mlawer, E. J., ~~S. J.~~ Taubman, ~~S. J.~~, ~~P. D.~~ Brown, ~~P. D.~~, ~~M. J.~~ Iacono, ~~M. J.~~, and ~~S. A.~~ Clough, ~~S. A.~~: (1997),  
800 Radiative transfer for inhomogeneous atmospheres: RRTM, a validated correlated-k model for the longwave,  
801 *J. Geophys. Res.*, 102(D14), 16663–16682, doi:10.1029/97JD00237, 1997.

802 ~~Nowlan, C. R., et al (2016), Nitrogen dioxide observations from the Geostationary Trace gas and Aerosol Sensor~~  
803 ~~Optimization (GeoTASO) airborne instrument: Retrieval algorithm and measurements during DISCOVER-~~  
804 ~~AQ Texas 2013, *Atmos. Meas. Tech.*, 9, 2647–2668, https://doi.org/10.5194/amt-9-2647-2016, 2016.~~

805 ~~Nowlan, C. R., (2018), Nitrogen dioxide and formaldehyde measurements from the GEOstationary Coastal and Air~~  
806 ~~Pollution Events (GEO-CAPE) Airborne Simulator over Houston, Texas, *Atmos. Meas. Tech.*, 11, 5941–~~  
807 ~~5964, https://doi.org/10.5194/amt-11-5941-2018, 2018.~~

808 Morrison, H., ~~J. A.~~ Curry, ~~J. A.~~, and ~~V. I.~~ Khvorostyanov, ~~V. I.~~: (2005), A new double-moment microphysics  
809 parameterization for application in cloud and climate models. Part 1: Description, *J. Atmos. Sci.*, 62, 1665–  
810 1677, doi:10.1175/JAS3446.1, 2005.

811 National Emissions Inventory Collaborative: (2019), 2016v1 Emissions Modeling Platform. Retrieved from  
812 <http://views.cira.colostate.edu/wiki/wiki/10202>, 2019.

813 Nault, B. A., ~~J. L.~~ Laughner, ~~J. L.~~, ~~P. J.~~ Wooldridge, ~~P. J.~~, ~~J. D.~~ Crouse, ~~J. D.~~, ~~J.~~ Dibb, ~~J.~~, ~~G.~~ Diskin, ~~G.~~, ~~J.~~ Peischl,  
814 ~~J.~~, ~~J. R.~~ Podolske, ~~J. R.~~, ~~I. B.~~ Pollack, ~~I. B.~~, ~~T. B.~~ Ryerson, ~~T. B.~~, ~~E.~~ Scheuer, ~~E.~~, ~~P. O.~~ Wennberg, ~~P. O.~~, and ~~R.~~  
815 ~~C.~~ Cohen, ~~R. C.~~: (2017), Lightening NOx emissions: Reconciling Measured and Modeled Estimates with  
816 Updated NOx Chemistry, *Geophys. Res. Lett.*, 44(18), 9479–9488, doi:10.1002/2017GL074436, 2017.

817 Nolte, C. G., ~~K. W.~~ Appel, ~~K. W.~~, ~~J. T.~~ Kelly, ~~J. T.~~, ~~P. V.~~ Bhave, ~~P. V.~~, ~~K. M.~~ Fahey, ~~K. M.~~, ~~J. L.~~ Collett, ~~J. L.~~, ~~L.~~  
818 ~~Zhang, L., and J. O.~~ Young, ~~J. O.~~: (2015), Evaluation of the Community Multiscale Air Quality (CMAQ)  
819 model v5.0 against size-resolved measurements of inorganic particle composition across sites in North  
820 America, *Geosci. Model Dev.*, 8(9), 2877–2892, doi:10.5194/gmd-8-2877-2015, 2015.

821 ~~Nowlan, C. R., Liu, X., Leitch, J. W., Chance, K., González Abad, G., Liu, C., Zoogman, P., Cole, J., Delker, T.,~~  
822 ~~Good, W., Murcray, F., Ruppert, L., Soo, D., Follette-Cook, M. B., Janz, S. J., Kowalewski, M. G., Loughner,~~  
823 ~~C. P., Pickering, K. E., Herman, J. R., Beaver, M. R., Long, R. W., Szykman, J. J., Judd, L. M., Kelley, P.,~~  
824 ~~Luke, W. T., Ren, X., and Al-Saadi, J. A.: Nitrogen dioxide observations from the Geostationary Trace gas~~  
825 ~~and Aerosol Sensor Optimization (GeoTASO) airborne instrument: Retrieval algorithm and measurements~~  
826 ~~during DISCOVER-AQ Texas 2013, *Atmos. Meas. Tech.*, 9, 2647–2668, https://doi.org/10.5194/amt-9-2647-~~  
827 ~~2016, 2016.~~

828 ~~Nowlan, C. R., Liu, X., Janz, S. J., Kowalewski, M. G., Chance, K., Follette-Cook, M. B., Fried, A., González Abad,~~  
829 ~~G., Herman, J. R., Judd, L. M., Kwon, H.-A., Loughner, C. P., Pickering, K. E., Richter, D., Spinei, E.,~~  
830 ~~Walega, J., Weibring, P., and Weinheimer, A. J.: Nitrogen dioxide and formaldehyde measurements from the~~  
831 ~~GEOstationary Coastal and Air Pollution Events (GEO-CAPE) Airborne Simulator over Houston, Texas,~~  
832 ~~*Atmos. Meas. Tech.*, 11, 5941–5964, https://doi.org/10.5194/amt-11-5941-2018, 2018.~~

833 ~~Otkin, J. A., Crouce, L. M., Case, J. L., Pierce, R. B., Harkey, M., Lenzen, A., Henderson, D. S., Adelman, Z.,~~  
834 ~~Nergui, T., and Hain, C. R.: Meteorological modeling sensitivity to parameterizations and satellite-derived~~  
835 ~~surface datasets during the 2017 Lake Michigan Ozone Study, *Atmos. Chem. Phys.*, EGUspere [preprint],~~  
836 ~~doi:10.5194/egusphere-2023-153, 2023.~~

837 Pierce, R. B., ~~T.~~ Schaack, ~~T.~~, ~~J. A.~~ Al-Saadi, ~~J. A.~~, ~~T. D.~~ Fairlie, ~~T. D.~~, ~~C.~~ Kittaka, ~~C.~~, ~~G.~~ Lingenfelter, ~~G.~~, ~~M.~~  
838 ~~Natarajan, M., J.~~ Olson, ~~J.~~, ~~A.~~ Soja, ~~A.~~, ~~T.~~ Zapotocny, ~~T.~~, ~~A.~~ Lenzen, ~~A.~~, ~~J.~~ Stobie, ~~J.~~, ~~D.~~ Johnson, ~~D.~~, ~~M. A.~~  
839 ~~Avery, M. A., G. W.~~ Sachse, ~~G. W.~~, ~~A.~~ Thompson, ~~A.~~, ~~R.~~ Cohen, ~~R.~~, ~~J. E.~~ Dibb, ~~J. E.~~, ~~D.~~ Rault, ~~D.~~, ~~R.~~ Martin,  
840 ~~R.~~, ~~J.~~ Szykman, ~~J.~~, and ~~J.~~ Fishman, ~~J.~~: (2007), Chemical data assimilation estimates of continental U.S. ozone  
841 and nitrogen budgets during the Intercontinental Chemical Transport Experiment-North America, *J. Geophys.*  
842 *Res. Atmos.*, 112(D12), doi:10.1029/2006JD007722, 2007.

843 Pleim, J. E.: (2007), A combined local and nonlocal closure model for the atmospheric boundary layer. Part I: Model  
844 description and testing, *J. Appl. Meteorol. Climatol.*, 46(9), 1383–1395, doi:10.1175/JAM2539.1, 2007.

Formatted: Font: Not Italic

Formatted: Font: Not Italic

Formatted: Font: Not Italic

Formatted: Font: Not Italic

Formatted: Font: Not Italic

Formatted: Font: Not Italic

Formatted: Font: Not Italic

Formatted: Font: Not Italic

Formatted: Font: Not Italic

Formatted: Font: Not Italic

Formatted: Font: Not Italic

845 [Ran, L., Pleim, J., Gilliam, R., Binkowski, F. S., Hogrefe, C., and Band, L.: Improved meteorology from an updated](#)  
846 [WRF/CMAQ modeling system with MODIS vegetation and albedo, \*J. Geophys. Res. Atmos.\*,121,2393–2415,](#)  
847 [doi:10.1002/2015JD024406, 2016](#)

848 Schwab, D. J., ~~G. A. Leshkevich, G. A., and G. C. Muhr, G. C.:~~ (1992), Satellite measurements of surface water  
849 temperature in the Great Lakes: Great Lakes Coastwatch, *J. Great Lakes Res.*, 18(2), 247-258,  
850 doi:10.1016/S0380-1330(92)71292-1, 1992.

851 Sexton, K., and ~~H. Westberg, H.:~~ (1980), Elevated Ozone Concentrations Measured Downwind of the Chicago-Gary  
852 Urban Complex, *J. Air Pollut. Control Assoc.*, 30(8), 911-914, doi:10.1080/00022470.1980.10465132, 1980.

853 Shindell, D., ~~J. C. I. Kuylenstierna, J. C. I., E. Vignati, E., R. Van Dingenen, R., M. Amann, M., Z. Klimont, Z., S.~~  
854 ~~C. Anenberg, S. C., N. Muller, N., G. Janssens-Maenhout, G., F. Raes, F., J. Schwartz, J., G. Faluvegi, G., L.~~  
855 ~~Pozzoli, L., K. Kupiainen, K., L. Höglund-Isaksson, L., L. Emberson, L., D. Streets, D., V. Ramanathan, V.,~~  
856 ~~K. Hicks, K., N. T. K. Oanh, N. T. K., G. Milly, G., M. Williams, M., V. Demkine, V., and D. Fowler, D.:~~  
857 (2012), Simultaneously Mitigating Near-Term Climate Change and Improving Human Health and Food  
858 Security, *Science*, 335(6065), 183-189, doi: 10.1126/science.1210026, 2012.

859 [Song, C.-K., Byun, D. W., Pierce, R. B., Alsaadi, J. A., Schaack, T. K., and Vukovich, F.: Downscale linkage of](#)  
860 [globalmodel output for regional chemical transport modeling: Method and general performance,\*J. Geophys.\*](#)  
861 [Res., 113, D08308, doi:10.1029/2007JD008951, 2008](#)

862 [Stroud, C. A., Ren, S., Zhang, J., Moran, M. D., Akingunola, A., Makar, P. A., Munoz-Alpizar, R., Leroyer, S.,](#)  
863 [Bélair, S., Sills, D., and Brook, J. R.: Chemical analysis of surface-level ozone exceedances during the 2015](#)  
864 [Pan American Games, \*Atmosphere\*, 11\(6\), 572, doi:10.3390/atmos11060572, 2020.](#)

865 Thompson, G., ~~P. R. Field, P. R., R. M. Rasmussen, R. M., and W. D. Hall, W. D.:~~ (2008), Explicit forecasts of  
866 winter precipitation using an improved bulk microphysics scheme. Part II: Implementation of a new snow  
867 parameterization, *Mon. Wea. Rev.*, 136(12), 5095-5115, doi:10.1175/2008MWR2387.1, 2008.

868 Thompson, G., ~~M. Tewari, M., K. Ikeda, K., S. Tessorndorf, S., C. Weeks, C., J. Otkin, J., and F. Kong, F.:~~ (2016),  
869 Explicitly-coupled cloud physics and radiation parameterizations and subsequent evaluation in WRF high-  
870 resolution convective forecasts, *Atmos. Res.*, 168, 92-104, doi:10.1016/j.atmosres.2015.09.005, 2016.

871 [US Environmental Protection Agency: CMAQ version 5.2., Zenodo \[software\], doi:10.5281/zenodo.1212601, 2018.](#)  
872 [US Environmental Protection Agency \(2021\).: 2017 National Emissions Inventory: January 2021 Updated Release,](#)  
873 [Technical Support Document, EPA-454/R-21-001, retrieved from](#)  
874 [https://www.epa.gov/sites/default/files/2021-02/documents/nei2017\\_tsd\\_full\\_jan2021.pdf, 2021.](#)

875 Vargas, M., ~~Z. Jiang, Z., J. Ju, J., and I. A. Csizsar, I. A.:~~ (2015), Real-time daily rolling weekly Green Vegetation  
876 Fraction (GVF) derived from the Visible Infrared Imaging Radiometer Suite (VIIRS) sensor onboard the  
877 SNPP satellite, 20<sup>th</sup> Conf. Satellite Meteorology and Oceanography, Phoenix AZ, Amer. Meteor. Soc., P210,  
878 retrieved from <https://ams.confex.com/ams/95Annual/webprogram/Paper259494.html>, 2015.

879 Wang, K., ~~Y. Zhang, Y., S. Yu, S., D. C. Wong, D. C., J. Pleim, J., R. Mathur, R., J. T. Kelly, J. T., and M. Bell, M.:~~  
880 (2021), A comparative study of two-way and offline coupled WRF v3.4 and CMAQ v5.0.2 over the  
881 contiguous US: performance evaluation and impacts of chemistry-meteorology feedbacks on air quality,  
882 *Geosci. Model Dev.*, 14, 7189-7221, doi: 10.5194/gmd-14-7189-2021, 2021.

883 Wagner, T. J., ~~Carnetzki, A. C., Christiansen, M., Pierce, R. B., Stanier, C. O., Dickens, A. F., and Eloranta, E. W.:~~  
884 ~~imothy J., et al.~~ "Observations of the Development and Vertical Structure of the Lake-Breeze Circulation  
885 during the 2017 Lake Michigan Ozone Study." *Journal of the Atmospheric Sciences*, *J. Atmos. Sci.*, 79(4), 4  
886 (2022): 1005-1020, doi:10.1175/JAS-D-20-0297.1, 2022.

887 Xiu, A., and ~~J. E. Pleim, J. E.:~~ (2001): Development of a land surface model. Part I: Application in a mesoscale  
888 meteorological model, *J. Appl. Meteor.*, 40(2), 192-209, doi:10.1175/1520-  
889 0450(2001)040<0192:DOALSM>2.0.CO;2, 2001.

Formatted: Font: Not Italic

Formatted: Font: Not Italic

Formatted: Font: Not Italic

Formatted: Font: Not Italic

Formatted: Font: Not Italic

Formatted: Font: Not Italic

Formatted: Font: Not Italic

Formatted: Font: Not Italic

Formatted: Font: Not Italic